Inorganic Chemistry

pubs.acs.org/IC Article

Synthesis of Palladium(II) Complexes via Michael Addition: Antiproliferative Effects through ROS-Mediated Mitochondrial Apoptosis and Docking with SARS-CoV-2

Jebiti Haribabu, Swaminathan Srividya,[#] Dharmasivam Mahendiran,[#] Dasararaju Gayathri, Vemula Venkatramu, Nattamai Bhuvanesh, and Ramasamy Karvembu*

Cite This: *Inorg. Chem.* 2020, 59, 17109−17122 Read Online

ACCESS | Metrics & More | Article Recommendations | Supporting Information

ABSTRACT: Metal complexes have numerous applications in the current era, particularly in the field of pharmaceutical chemistry and catalysis. A novel synthetic approach for the same is always a beneficial addition to the literature. Henceforth, for the first time, we report the formation of three new Pd(II) complexes through the Michael addition pathway. Three chromone-based thiosemicarbazone ligands (SVSL1−SVSL3) and Pd(II) complexes (**1**−**3**) were synthesized and characterized by analytical and spectroscopic tools. The Michael addition pathway for the formation of complexes was confirmed by spectroscopic studies. Distorted square planar structure of complex **2** was confirmed by single-crystal X-ray diffraction. Complexes **1**−**3** were subjected to DNA- and BSA-binding studies. The complex with cyclohexyl substituent on the terminal N of thiosemicarbazone (**3**) showed the highest binding efficacy toward these biomolecules, which was further understood through molecular docking studies. The anticancer potential of these complexes was studied preliminarily by using MTT assay in cancer and normal cell lines along with the benchmark drugs (cisplatin, carboplatin, and gemcitabine). It was found that complex **3** was highly toxic toward MDA-MB-231 and AsPC-1 cancer cells with IC_{50} values of 0.5 and 0.9 μM, respectively, and was more efficient than the standard drugs. The programmed cell death mechanism of the complexes in MDA-MB-231 cancer cells was confirmed. Furthermore, the complexes induced apoptosis via ROS-mediated mitochondrial signaling pathway. Conveniently, all the complexes showed less toxicity (≥50 μM) against MCF-10a normal cell line. Molecular docking studies were performed with VEGFR2, EGFR, and SARS-CoV-2 main protease to illustrate the binding efficiency of the complexes with these receptors. To our surprise, binding potential of the complexes with SARS-CoV-2 main protease was higher than that with chloroquine and hydroxychloroquine.

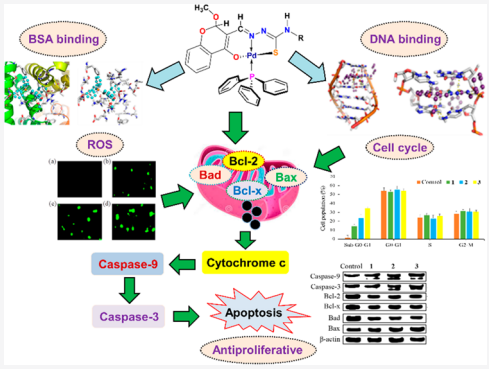

INTRODUCTION

Cancer, since its discovery, has been a life-threatening disease globally. It marks the unmanageable growth of abnormal cells that can colonize and disrupt the tissues.[1] The usage of metal complexes as drugs lingers strongly, either unaided or in combination with the other drugs, even though the side effects and development of drug resistance are highly likely.[2] Currently, Pt therapeutics (cisplatin, carboplatin, oxaliplatin, etc.) are in use for almost 50−70% of cancer therapy. However, their dosage is restrained due to their unsympathetic side effects such as nausea, vomiting, loss of sensation in the extremities, and nephrotoxicity.[3,4] Pd(II) complexes are noteworthy alternatives for the treatment of cancer because of their structural and thermodynamic similarities to Pt(II) complexes.[5−7] There have been numerous reports on Pd(II) complexes with potential anticancer properties against various cancer cell lines (lung, prostate, etc.); some are showing better activity (predominantly in *in vitro* system) than their Pt(II) counterparts.[8−11] Pd(II) complexes have shown remarkable antiproliferative effects on human breast cancer including tumor cell lines that are resistant to cisplatin, and also displayed good antimycobacterial effects.[12−15]

Thiosemicarbazones (>C═N−NH−C(S)−N<) (TSCs) have evolved as an imperative class of Schiff base ligands that are structurally appealing and biologically active candidates. Triapine, which is presently in phase I clinical trial against cancer cell lines, and thiacetazone, which has proved beneficial for the treatment of tuberculosis, are some drugs that have highlighted the biological activities of this class of compounds.[16,17] Heterocyclic TSCs have been portrayed as

Received: August 8, 2020
Published: November 24, 2020

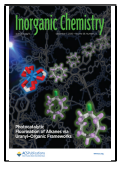

https://dx.doi.org/10.1021/acs.inorgchem.0c02373
Inorg. Chem. 2020, 59, 17109−17122

compounds that not only target the ribonucleotide reductase but also other intracellular molecules such as N-myc downstream-regulated gene-1 (NDRG1) and DNA topoisomerase IIa (top2a).[18] Such properties of TSCs fascinated the researchers to explore their coordination behavior with metal ions.[18−21] In many cases, coordination of these ligands to metal ions increases their biological activity, proposing that complexation could be a significant approach for dose reduction. The coordination behavior of TSCs and medicinal applications of their metal complexes have been established briefly in the literature.[22−27]

Chromones are compounds which contain a γ-pyrone nucleus fused to a phenyl ring at the fifth and sixth positions. Chromones and flavones have played a vital role in the human diet. Numerous biologically active molecules derived from natural sources contain a chromone moiety as their core.[28−31] These compounds have attracted the pharmaceutical industries to a large extent owing to their antioxidant, antitumor and antibacterial activities.[32−34] Besides these, several chromone derivatives have been used as antimicrobial, DNA-binding, DNA-cleavage, anticancer, antiallergic, neuroprotective, and pesticidal agents.[28−44] Although the appeal of chromones and their derivatives is widespread, the literature still lacks knowledge about their importance in coordination chemistry. Our group has been meticulously involved in studying the coordination behavior of heterocyclic TSCs with Ni(II), Cu(II), Zn(II), Pd(II), and Ru(II) and its influence on the biomolecular interactions and anticancer activity against various cancer and normal cell lines.[45−56] Most of these complexes induced cell death through apoptosis.

The broadcast of severe acute respiratory syndrome coronavirus 2 (SARS-CoV-2), i.e., COVID-19, has been declared as pandemic by the World Health Organization (WHO) and has affected hundreds of countries in a matter of weeks. A global response to prepare health systems is a priority.[57] Hence, we have extended our research to understand the interactions between the present Pd(II) complexes and the SARS-CoV-2 main protease through molecular docking (MD) studies. MD studies with DNA, BSA protein, vascular epithelial growth factor receptor (VEGFR2), and epithelial growth factor receptor (EGFR) have also been carried out to learn the mechanism of action of the complexes through which they exhibit a cytotoxic effect.

The biological properties of Pd, heterocyclic TSCs, and functionalized chromones have motivated us to develop better anticancer agents than the ones obtained earlier. Herein, we report the synthesis of the novel Pd(II) complexes bearing chromone TSC through Michael addition. The compounds were well-characterized by analytical, spectroscopic, and single-crystal X-ray diffraction methods and were evaluated to know their biomolecular (DNA, protein, VEGFR2, EGFR, and SARS-CoV-2 main protease) interactions and anticancer potential. To the best of our knowledge, this is the first report on the synthesis of Pd(II) complexes through Michael addition.

EXPERIMENTAL SECTION

Materials and Methods. Analytical-grade chemicals and solvents were purchased from commercial suppliers (Sigma-Aldrich, Promega, Biolegend, BD Biosciences, and Alfa Aesar) and used as received. The melting points were determined on a Lab India instrument and are uncorrected. Elemental analyses were carried out using a PerkinElmer instrument. FT-IR spectra were obtained as KBr pellets using a Nicolet-iS5 spectrophotometer. UV−visible (UV−vis) spectra were recorded using a Shimadzu-2600 spectrophotometer. Emission spectra were recorded on a Jasco V-630 spectrophotometer using 5% DMSO in buffer as solvent. NMR spectra were recorded in $CDCl_3$/DMSO-d_6 solvent by using TMS as an internal standard on a Bruker 500/400 MHz spectrometer. ESI-MS spectra were obtained using a Waters ZQ 4000 or Bruker maXis impact mass spectrometer. MALDI mass spectra were recorded on a 4800 Applied Bio System mass spectrometer. Single-crystal X-ray data collections for the ligand (SVSL1) and Pd(II) complex (**2**) were done at 110 K with a APEX Kα diffractometer using graphite monochromated Mo Kα (λ = 0.70173 Å) radiation. The structural solution was obtained readily using XT/XS in APEX2[58,59] and refined by full matrix least-squares on F^2 using Olex2.[60] Stability of the Pd(II) complexes was determined in 1% aqueous DMSO by recording their UV−vis spectra over a period of 24 h at room temperature.[61] The ROS level was calculated in MDA-MB-231 cancer cells using fluorescent probe 2′,7′-dichlorodihydrofluorescein diacetate (DCFH-DA). Hoechst and acridine orange (AO)/ethidium bromide (EB) staining assays were performed to analyze the morphological changes in MDA-MB-231 cancer cells.

Synthesis of the Chromone TSCs (SVSL1−SVSL3). Chromone-appended TSC ligands (SVSL1−SVSL3) were synthesized from the reactions between 3-formylchromone (1.74 g, 10 mmol) and thiosemicarbazide or 4-ethylthiosemicarbazide or 4-cyclohexylthiosemicarbazide (0.91−1.73 g, 10 mmol) in ethanol in the presence of acetic acid (2−4 drops). The mixture was refluxed for 4 h. Upon cooling the solution in deep freezer, a white precipitate was formed, which was then filtered. The solid was washed with cold ethanol and dried in *vacuum*. The white crystals of SVSL1 suitable for X-ray diffraction were obtained from slow evaporation of the ligand solution (1:3 DMF−$CHCl_3$ mixture).

(E)-2-((4-Oxo-4H-chromen-3-yl)methylene)-hydrazinecarbothioamide (SVSL1). Thiosemicarbazide (0.91 g, 10 mmol) was used. Yield: 2.27 g, 94%. White solid. Mp: 221 °C. Anal. Calcd for $C_{11}H_9N_3O_2S$ (%): C, 53.43; H, 3.67; N, 16.99; S, 12.97. Found: C, 53.37; H, 3.60; N, 17.15; S, 12.84. UV−vis (DMSO): λ_{max}, nm 258, 329 ($\pi \rightarrow \pi^*$ and n $\rightarrow \pi^*$). FT-IR (KBr): υ, cm^{-1} 3379 (N−H), 3243 (H−N−C═S), 1641 (C═O), 1517 (C═N), 1341 (C−O), 1226 (C═S). ^{1}H NMR (400 MHz, DMSO-d_6): δ, ppm 11.54 (s, 1H, N−NH−CS), 9.14 (s, 1H, CH═N), 8.25 (s, 1H, N**H**$_2$), 8.18 (s, 1H, O−CH), 8.10 (d, J = 7.6 Hz, 2H, N**H**$_2$ and aromatic), 7.83 (t, J = 7.6 Hz, 1H, aromatic), 7.70 (d, J = 8.4 Hz, 1H, aromatic), 7.53 (t, J = 7.6 Hz, 1H, aromatic). ^{13}C NMR (100 MHz, DMSO-d_6): δ, ppm 178.4 (C═S), 175.3 (C═O), 156.1 (C−O), 155.6 (C═N), 135.0, 134.6, 126.5, 125.6, 123.7, 119.1, 118.7 (aromatic carbons of chromone moiety). ESI-MS m/z [Found (Calcd)]: 248.0401 (248.0494) {$[M + H^+]^+ \equiv [C_{11}H_{10}N_3O_2S]^+$}.

(E)-N-Ethyl-2-((4-oxo-4H-chromen-3-yl)methylene)-hydrazinecarbothioamide (SVSL2). 4-Ethylthiosemicarbazide (1.19 g, 10 mmol) was used. Yield: 2.47 g, 90%. White solid. Mp: 196 °C. Anal. Calcd for $C_{13}H_{13}N_3O_2S$ (%): C, 56.71; H, 4.76; N, 15.26; S, 11.64. Found: C, 56.60; H, 4.89; N, 15.39; S, 11.55. UV−vis (DMSO): λ_{max}, nm 259, 328 ($\pi \rightarrow \pi^*$ and n $\rightarrow \pi^*$). FT-IR (KBr): υ, cm^{-1} 3363 (N−H), 3239 (H−N−C═S), 1634 (C═O), 1541 (C═N), 1344 (C−O), 1221 (C═S). ^{1}H NMR (400 MHz, DMSO-d_6): δ, ppm 11.50 (s, 1H, N−NH−CS), 9.08 (s, 1H, CH═N), 8.59 (t, J = 5.8 Hz, 1H, N**H**−C_2H_5), 8.15 (s, 1H, O−CH), 8.09 (dd, J = 8.0, 1.6 Hz, 1H, aromatic), 7.82 (td, J = 8.7, 1.7 Hz, 1H, aromatic), 7.68 (d, J = 8.1 Hz, 1H, aromatic), 7.52 (td, J = 7.6, 0.9 Hz, 1H, aromatic), 2.50 (p, J = 6.8 Hz, 2H, NH−C**H**$_2$), 1.14 (t, J = 7.1 Hz, 3H, CH_2−C**H**$_3$). ^{13}C NMR (100 MHz, DMSO-d_6): δ, ppm 177.0 (C═S), 175.3 (C═O), 156.1 (C−O), 155.4 (C═N), 135.0, 134.2, 126.5, 125.6, 123.7, 119.1, 118.7 (aromatic carbons of chromone moiety), 38.7, 15.0 (aliphatic carbons of ethyl group). ESI-MS m/z [Found (Calcd)]: 298.0610 (298.0626) {$[M + Na^+]^+ \equiv [C_{13}H_{13}N_3O_2SNa]^+$}.

(E)-N-Cyclohexyl-2-((4-oxo-4H-chromen-3-yl)methylene)-hydrazinecarbothioamide (SVSL3). 4-Cyclohexylthiosemicarbazide (1.73 g, 10 mmol) was used. Yield: 2.73 g, 83%. White solid. Mp: 210 °C. Anal. Calcd for $C_{17}H_{19}N_3O_2S$ (%): C, 61.98; H, 5.81; N, 12.76; S, 9.73. Found: C, 61.86; H, 5.94; N, 12.61; S, 9.89. UV−vis (DMSO):

https://dx.doi.org/10.1021/acs.inorgchem.0c02373
Inorg. Chem. 2020, 59, 17109−17122

λ_{max}, nm 264, 339 ($\pi \rightarrow \pi^*$ and n $\rightarrow \pi^*$). FT-IR (KBr): υ, cm^{-1} 3354 (N−H), 3230 (H−N−C═S), 1640 (C═O), 1527 (C═N), 1320 (C−O), 1255 (C═S). ^{1}H NMR (400 MHz, DMSO-d_6): δ, ppm 11.53 (s, 1H, N−NH−CS), 9.18 (s, 1H, CH═N), 8.18 (s, 1H, O−CH), 8.10 (d, J = 7.6 Hz, 2H, N**H**−C_6H_{11} and aromatic), 7.84 (t, J = 7.8 Hz, 1H, aromatic), 7.71 (d, J = 8.4 Hz, 1H, aromatic), 7.53 (t, J = 7.6 Hz, 1H, aromatic), 4.23−4.15 (m, 1H, NH−cyclohexyl C**H**), 1.88 (d, J = 11.0 Hz, 2H, cyclohexyl), 1.74 (d, J = 12.4 Hz, 2H, cyclohexyl), 1.62 (d, J = 12.2 Hz, 1H, cyclohexyl), 1.40 (dd, J = 23.9, 11.7 Hz, 2H, cyclohexyl), 1.28 (dd, J = 25.2, 12.5 Hz, 2H, cyclohexyl), 1.12 (dd, J = 24.5, 12.3 Hz, 1H, cyclohexyl). ^{13}C NMR (100 MHz, DMSO-d_6): δ, ppm 176.0 (C═S), 175.2 (C═O), 156.1 (C−O), 155.7 (C═N), 135.0, 134.5, 126.4, 125.6, 123.7, 119.1, 118.6 (aromatic carbons of chromone moiety), 53.1, 32.3, 25.6, and 25.4 (aliphatic carbons of cyclohexyl group). ESI-MS m/z [Found (Calcd)]: 330.1226 (330.1276) {[M + H^+]$^+$ ≡ [$C_{17}H_{20}N_3O_2S$]$^+$}.

Synthesis of the Pd(II) Complexes (1−3). [$PdCl_2(PPh_3)_2$] (350 mg, 0.5 mmol) was dissolved in methanol (20 mL), and solution of the corresponding chromone-based TSC ligand (123−164 mg, 0.5 mmol) in methanol (10 mL) was added. The mixture was stirred at room temperature for 10 min under N_2 atmosphere to form an orange precipitate, which was separated from the solution by filtration, washed with cold methanol and hexane, and dried in *vacuum*. The orange crystals of complex **2** suitable for single-crystal X-ray diffraction were obtained by recrystallization from its CH_2Cl_2−DMF (3:1) solution.

*[Pd(SVSL1-OCH$_3$)(PPh$_3$)] (**1**).* SVSL1 (123 mg, 0.5 mmol) was used. Yield: 0.53 g, 85%. Orange solid. Mp: 228 °C. Anal. Calcd for $C_{30}H_{26}N_3O_3PPdS$ (%): C, 55.78; H, 4.06; N, 6.50; S, 4.96. Found: C, 55.64; H, 4.20; N, 6.61; S, 4.81. UV−vis (DMSO): λ_{max}, nm 259, 330 ($\pi \rightarrow \pi^*$ and n $\rightarrow \pi^*$), 370, 384 (LMCT). FT-IR (KBr): υ, cm^{-1} 3370 (N−H), 1580 (C═C−O), 1472 (C═N), 1335 (C−O), 1176 (C−S), 1436, 1096, 759 (for PPh_3). ^{1}H NMR (500 MHz, $CDCl_3$): δ, ppm 7.73 (d, J = 14.0 Hz, 1H, CH═N), 7.71−7.65 (m, 6H, aromatic), 7.52−7.46 (m, 3H, aromatic), 7.42 (t, J = 6.8 Hz, 6H, aromatic), 7.20 (t, J = 7.6 Hz, 1H, aromatic), 6.93 (d, J = 8.0 Hz, 1H, aromatic), 6.72 (d, J = 7.7 Hz, 1H, aromatic), 6.66 (t, J = 7.5 Hz, 1H, aromatic), 5.74 (s, 1H, OCH), 4.49 (s, 2H, terminal NH_2), 3.47 (s, 3H, OCH_3). ^{13}C NMR (125 MHz, $CDCl_3$): δ, ppm 166.9 (C−S), 159.7 (C═C−O), 153.8 (C−O), 146.6 (C═N), 134.5, 131.0, 130.9, 129.7, 129.3, 128.6, 125.7, 122.0, 121.2, 116.6, 102.4 (aromatic carbons of chromone moiety and triphenylphosphine), 97.5 (OCH), 55.3 (OCH_3). DEPT-135 (125 MHz, $CDCl_3$): δ, ppm 146.4 (C═N), 134.5, 131.1, 131.0, 128.6, 125.7, 121.2, 116.6, 102.3 (+ peaks, aromatic carbons of chromone moiety and triphenylphosphine), 55.3 (+ peak, OCH_3). ^{31}P NMR (203 MHz, $CDCl_3$): δ, ppm 26.0 (1P). ESI-MS m/z [Found (Calcd)]: 614.0374 (614.0283) {[M − MeOH]$^+$ ≡ [$C_{29}H_{23}N_3O_2PPdS$]$^+$}.

*[Pd(SVSL2-OCH$_3$)(PPh$_3$)] (**2**).* SVSL2 (137 mg, 0.5 mmol) was used. Yield: 0.55 g, 83%. Orange solid. Mp: 208 °C. Anal. Calcd for $C_{32}H_{30}N_3O_3PPdS$ (%): C, 57.02; H, 4.49; N, 6.23; S, 4.76. Found: C, 57.14; H, 4.65; N, 6.41; S, 4.69. UV−vis (DMSO): λ_{max}, nm 263, 341 ($\pi \rightarrow \pi^*$ and n $\rightarrow \pi^*$), 386, 396 (LMCT). FT-IR (KBr): υ, cm^{-1} 3360 (N−H), 1604 (C═C−O), 1499 (C═N), 1349 (C−O), 1197 (C−S), 1453, 1056, 750 (for PPh_3). ^{1}H NMR (500 MHz, $CDCl_3$): δ, ppm 7.73 (d, J = 14.1 Hz, 1H, CH═N), 7.66−7.58 (m, 6H, aromatic), 7.46−7.39 (m, 3H, aromatic), 7.35 (td, J = 16.8, 2.2 Hz, 6H, aromatic), 7.11 (td, J = 16.9, 1.7 Hz, 1H, aromatic), 6.85 (d, J = 8.0 Hz, 1H, aromatic), 6.65 (dd, J = 7.7, 1.6 Hz, 1H, aromatic), 6.59 (t, J = 7.4 Hz, 1H, aromatic), 5.68 (s, 1H, OCH), 4.23 (t, J = 5.3 Hz, 1H, N**H**−C_2H_5), 3.40 (s, 3H, OCH_3), 3.21 (p, J = 7.1, 2H, NH−C**H**$_2$CH$_3$), 1.08 (t, J = 7.2 Hz, 3H, CH_2−C**H**$_3$). ^{13}C NMR (125 MHz, $CDCl_3$): δ, ppm 166.2 (C−S), 159.0 (C═C−O), 153.7 (C−O), 146.1 (C═N), 134.5, 130.9, 130.7, 129.9, 129.4, 128.5, 125.6, 121.1, 116.5, 102.4 (aromatic carbons of chromone moiety and triphenylphosphine), 97.4 (OCH), 55.2 (OCH_3), 41.3, 14.9 (aliphatic carbons of ethyl group). DEPT-135 (125 MHz, $CDCl_3$): δ, ppm 146.1 (C═N), 134.5, 131.0, 130.7, 128.5, 125.6, 121.1, 116.5, 102.4 (+ peaks, aromatic carbons of chromone moiety and triphenylphosphine), 55.3 (+ peak, OCH_3), 41.3 (− peak, aliphatic carbon of ethyl group), 14.9 (+ peak, aliphatic carbon of ethyl group). ^{31}P NMR (203 MHz, $CDCl_3$): δ, ppm 26.1 (1P). MALDI mass m/z [Found (Calcd)]: 642.0500 (642.0596) {[M − MeOH]$^+$ ≡ [$C_{31}H_{27}N_3O_2PPdS$]$^+$}.

*[Pd(ONS-SVSL3-OCH$_3$)(PPh$_3$)] (**3**).* SVSL3 (164 mg, 0.5 mmol) was used. Yield: 0.57 g, 79%. Orange solid. Mp: 225 °C. Anal. Calcd for $C_{36}H_{36}N_3O_3PPdS$ (%): C, 59.38; H, 4.98; N, 5.77; S, 4.40. Found: C, 59.43; H, 5.11; N, 5.91; S, 4.57. UV−vis (DMSO): λ_{max}, nm 274, 333 ($\pi \rightarrow \pi^*$ and n $\rightarrow \pi^*$), 373, 389 (LMCT). FT-IR (KBr): υ, cm^{-1} 3349 (N−H), 1600 (C═C−O), 1492 (C═N), 1349 (C−O), 1201 (C−S), 1434, 1063, 745 (for PPh_3). ^{1}H NMR (500 MHz, $CDCl_3$): δ, ppm 7.79 (d, J = 14.1 Hz, 1H, CH═N), 7.69−7.50 (m, 6H, aromatic), 7.48−7.30 (m, 3H, aromatic), 7.41 (t, J = 7.4 Hz, 6H, aromatic), 7.18 (t, J = 7.6 Hz, 1H, aromatic), 6.92 (d, J = 8.1 Hz, 1H, aromatic), 6.72 (d, J = 7.7 Hz, 1H, aromatic), 6.65 (t, J = 7.4 Hz, 1H, aromatic), 5.75 (s, 1H, OCH), 4.30 (d, J = 7.6 Hz, 1H, N**H**−C_6H_{11}), 3.53 (dd, J = 17.5, 9.9 Hz, 1H, cyclohexyl), 3.47 (s, 3H, OCH_3), 2.03 (t, J = 11.2 Hz, 2H, cyclohexyl), 1.71−1.61 (m, 2H, cyclohexyl), 1.57 (d, J = 12.5 Hz, 1H, cyclohexyl), 1.33 (dd, J = 24.2, 12.1 Hz, 2H, cyclohexyl), 1.21−1.04 (m, 3H, cyclohexyl). ^{13}C NMR (125 MHz, $CDCl_3$): δ, ppm 165.1 (C−S), 158.8 (C═C−O), 153.7 (C−O), 145.8 (C═N), 134.5, 130.9, 130.6, 129.9, 129.5, 128.5, 125.5, 122.2, 121.1, 116.5, 102.4 (aromatic carbons of chromone moiety and triphenylphosphine), 97.4 (OCH), 55.2 (OCH_3), 54.8, 33.2, 25.7, 24.8 (cyclohexyl carbons). DEPT-135 (125 MHz, $CDCl_3$): δ, ppm 145.8 (C═N), 134.5, 134.3, 130.9, 130.6, 128.6, 128.5, 125.6, 121.2, 116.5, 102.5 (+ peaks, aromatic carbons of chromone moiety and triphenylphosphine), 55.2 (+ peak, OCH_3), 54.8 (+ peak, cyclohexyl carbon), 33.2, 25.8, 24.8 (− peaks, cyclohexyl carbons). ^{31}P NMR (203 MHz, $CDCl_3$): δ, ppm 26.1 (1P). ESI-MS m/z [Found (Calcd)]: 696.1086 (696.1066) {[M − MeOH]$^+$ ≡ [$C_{35}H_{33}N_3O_2PPdS$]$^+$}.

DNA and Protein Binding Studies. Binding ability of the Pd(II) complexes with calf-thymus DNA (CT DNA) was evaluated using electronic absorption titration, ethidium bromide (EB) displacement and viscosity experiments. Binding of the complexes with bovine serum albumin (BSA) protein was studied by UV−vis and fluorescence spectroscopy. The detailed experimental procedures are provided in the Supporting Information.

Molecular Docking Studies. Molecular docking was performed for the Pd(II) complexes using AutoDock Tools (ADT) version 1.5.6 and AutoDock version 4.2.5 software[62] with the receptor binding sites of DNA hexamer d(CGATCG)$_2$ (Protein Data Bank (PDB) ID: 1Z3F),[63] BSA (PDB ID: 3V03),[64] and SARS-CoV-2 main protease (PDB ID: 6Y2F)[65] obtained from the Protein Data Bank (http://www.rcsb.org/pdb).[66] Schrodinger Glide[67] was used for MD studies of the complexes with VEGFR2 and EGFR enzymes.[68,69]

Antiproliferative Activity. Complexes **1**−**3** and positive controls (cisplatin, carboplatin, and gemcitabine) were dissolved in DMSO (10 mM) to prepare stock solutions for antiproliferative assay. Human pancreatic (PANC-1), human breast adenocarcinoma (MCF-7), epithelial human breast (MDA-MB-231) and nontumorigenic epithelial breast (MCF-10a) cells were maintained in Dulbecco's modified Eagle's medium (DMEM), and pancreatic carcinoma (AsPC-1) cells were maintained in Roswell Park Memorial Institute (RPMI-1640) medium, with 10% fetal bovine serum (FBS). The amount of DMSO was maintained below 0.5% (v/v) so that it does not have any influence on the cancer cell proliferation results. The cancer and normal cells (1.5×10^4) were treated with the test compounds (0−100 μM) under 5−6% CO_2 atmosphere at 37 °C and incubated for 72 h. A blank was also conducted and labeled as control. MTT reagent [5 mg/mL, 10 μL] was then added to each of the cell lines. After 2 h of incubation, 100 μL of DMSO was added and the absorbance of the formazan product was measured at 570 nm using a multi-well ELISA plate reader. The formazan product formation is directly proportional to the viability of the cells measured by Trypan blue staining.[70]

Nuclear Morphological Changes. MDA-MB-231 cancer cells in DMEM (5×10^5) were seeded in dishes (35 mm diameter), attached overnight, and incubated at 37 °C under 5% CO_2. The corresponding complex (25 μM) was then added to each well. Then, the dishes were

https://dx.doi.org/10.1021/acs.inorgchem.0c02373
Inorg. Chem. 2020, 59, 17109−17122

Scheme 1. Synthesis of the Chromone TSC Ligands

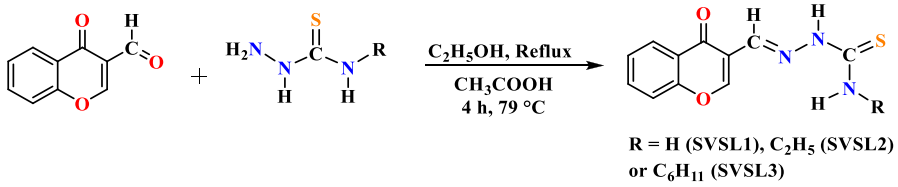

incubated at 37 °C under 5% CO_2 for 48 h. Upon completion of the incubation, the wells were washed 3 times with PBS after removing the culture media. The cells were then stained with 4′,6-diamidino-2-phenylindole (DAPI) and imaged by fluorescence microscopy.

Cell Cycle Analysis. The detailed procedure adopted for the study is provided in the Supporting Information. Cell cycle analysis was carried out using a fluorescence-activated cell sorter (FACS) [Becton Dickinson (BD) cell analyzer] at the FL2 channel (595 nm), and the distributions of cells in various cell cycle phases were determined from the histogram generated by the Cell Quest Pro software (BD Biosciences, San Jose, CA).

Western Blot Analysis. MDA-MB-231 cancer cells (3×10^5) were seeded into 6-well plates for 48 h and incubated with the complexes (25 μM) in the presence of 10% FBS. Then, the cells were collected using trypsinization and washed 3 times with PBS, lysed in cell lysis buffer and 2 μg/mL leupeptin, and then centrifuged at 10000 rpm for 10 min at 4 °C. The protein concentration of the supernatant was determined by bicinchoninic acid (BCA) assay. The samples were subjected to SDS-polyacrylamide gel electrophoresis (SDS-PAGE) with 10% resolving gel. Gels were then exchanged by poly(vinylidene difluoride) membranes (Millipore) and obstructed with 5% non-fat milk in Tris-buffered saline (TBST, 0.1% Tween 20) buffer for 1 h. After the membranes were incubated with primary antibodies at 1:2000 dilutions in 5% non-fat milk overnight at 37 °C, the membranes were washed 4 times with TBST buffer. Then, the secondary antibodies were conjugated with horseradish peroxidase at 1:2000 dilutions for 1 h at room temperature and afterward washed 4 times with TBST buffer. To evaluate the presence of comparable quantity of proteins in every lane, the membranes were stripped finally to detect β-actin followed by visualization with the enhanced chemiluminescence (ECL) PLUS detection reagents following the manufacturer's procedure (Amersham Biosciences).

RESULTS AND DISCUSSION

Synthesis of the Ligands and Complexes. The chromone TSC ligands (SVSL1−SVSL3) were synthesized by reacting 3-formylchromone with (un)substituted thiosemicarbazide in ethanol in the presence of acetic acid (Scheme 1). The ligands were air-stable, soluble in dimethylformamide and dimethyl sulfoxide, and insoluble in methanol, chloroform, acetonitrile, benzene, and water.

The Pd(II) complexes of the general formula [Pd(ONS-SVSL-OCH_3)(PPh_3)] were synthesized from the reactions of ligands SVSL1−SVSL3 with [$PdCl_2(PPh_3)_2$] in methanol under inert condition (Scheme 2). Complexes **1**−**3** were obtained in good yields as orange solids. They were air- and light-stable and soluble in most of the organic solvents. The analytical data of ligands and their complexes were in good agreement with the molecular formulas suggested.

Spectroscopic Confirmation of the Structures. The ligands displayed two bands in their UV−vis absorption spectra in the regions 258−264 and 328−339 nm, which were characteristic of $\pi \rightarrow \pi^*$ and n $\rightarrow \pi^*$ transitions, respectively. In contrast, the complexes depicted four bands. In addition to the intraligand transitions appeared around 259−274 and 330−341 nm, two new bands were seen in the regions 370−

Scheme 2. Synthesis of the Pd(II) Complexes

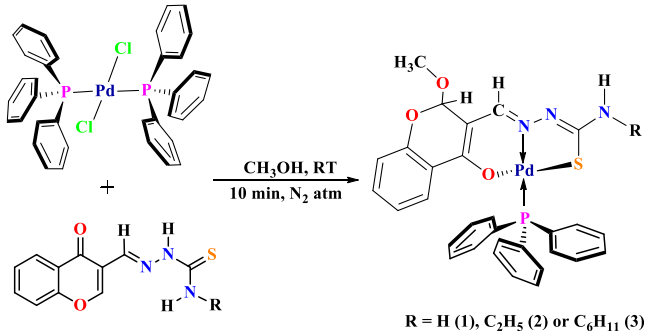

386 and 384−396 nm, which corresponded to ligand to metal charge transfer transitions (LMCT).[69,70]

FT-IR spectra of the ligands exhibited bands at 3354−3377 and 3230−3249 cm^{-1}, which were assigned to terminal and thioamide NH groups, respectively. Although the terminal NH stretching frequency (3349−3360 cm^{-1}) remained in the spectra of the complexes, thioamide NH stretching frequency disappeared. In the spectra of the complexes, the three characteristic stretching frequencies (C═O, C═N, and C═S) decreased compared to those of the ligands, which suggested that the ligands coordinated to Pd(II) ion through carbonyl oxygen, imine nitrogen, and thiocarbonyl sulfur atoms. A new band was observed around 1580−1604 cm^{-1}, which was characteristic of C−O−C stretching. The appearance of this band preliminarily indicated that the complex formation might have happened through Michael addition. The bands around 1434−1453, 1056−1096, and 745−759 cm^{-1} corresponded to the stretching frequencies of triphenylphosphine moiety.

The ^{1}H NMR spectra of SVSL1−SVSL3 mainly exhibited four sets of signals (Figures S1, S3, and S5). The first set of signals appeared at 11.50−11.54 and 8.10−8.25 ppm corresponded to thioamide and terminal NH protons, respectively. In the spectra of the complexes (Figures S7, S11, and S15), a signal due to the thioamide NH proton disappeared and that of terminal NH proton was shifted to a lower chemical shift value (4.23−4.49 ppm) when compared to the corresponding free ligands. Second, an azomethine proton was observed around 9.08−9.80 ppm as a singlet in the spectra of the ligands, whereas the same proton was observed at 7.73−7.79 ppm as a doublet in the spectra of the complexes. Third, a signal located at 8.10−8.59 ppm in the spectra of the ligands was due to the OCH proton of the chromone moiety, which was shifted upfield (5.60−5.75 ppm) upon coordination of the ligands. Furthermore, a new signal appeared at 3.40−3.47 ppm in the spectra of the complexes was assigned to the OCH_3 protons, which confirmed that the Michael addition had occurred during the complex formation. Finally, the last set of signals corresponding to the aromatic protons were observed around 7.52−8.09 ppm in the spectra of the ligands, whereas

https://dx.doi.org/10.1021/acs.inorgchem.0c02373
Inorg. Chem. 2020, 59, 17109−17122

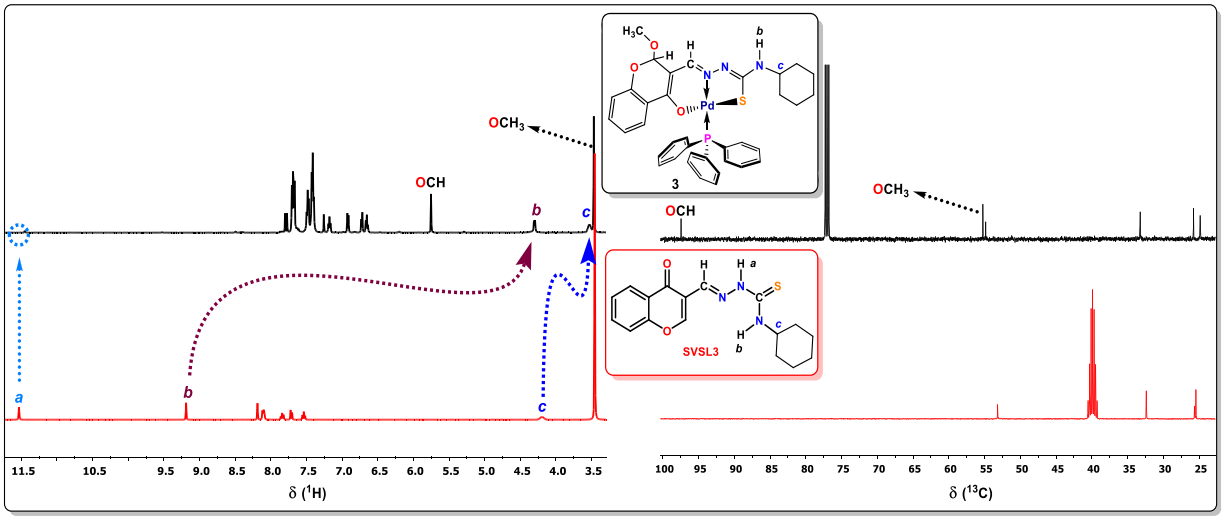

Figure 1. ^{1}H and ^{13}C NMR spectral evidence for the transformation of the chromone TSC (SVSL3) into **3**.

they were seen around 6.59−7.71 ppm after coordination of the ligands. The ethyl protons of SVSL2 and **2** were observed in the regions 2.50−1.14 and 3.21−1.08 ppm, respectively. The cyclohexyl protons of SVSL3 and complex **3** were detected at 4.23−1.22 and 4.30−1.04 ppm, respectively.

In the ^{13}C NMR spectra of the ligands, the peaks due to C═S, C═O, C−O, and C═N carbons appeared at 176.0−178.4, 175.2−175.3, 156.1, and 155.4−155.7 ppm, respectively (Figures S2, S4, and S6). The same carbon signals were observed at lower chemical shift values (165.1−166.9, 158.8−159.7, 153.7−153.8, and 145.8−146.6 ppm) in the spectra of the complexes (Figures S8, S12, and S16). Two new signals were observed in the spectra of the complexes at 97.4 and 55.2 ppm, which were due to the O−CH and OCH_3 carbons, respectively, confirming that the Michael addition had happened in the chromone (C2) moiety. The ^{31}P NMR spectra of the complexes showed a signal at 26.0−26.1 ppm as a singlet, which was characteristic of phosphorus atom of the coordinated triphenylphosphine (Figures S10, S14, and S18, Table S1). ^{1}H and ^{13}C NMR spectral evidence for the formation of complex **3** from SVSL3 is shown in Figures 1 and S19. All the ligands and complexes were also characterized by mass spectrometry (Figures S20−25).

Molecular Structures and Validation of Michael Addition. Crystal structures of SVSL1 and complex **2** with the atomic labeling scheme are displayed in Figures 2 and 3,

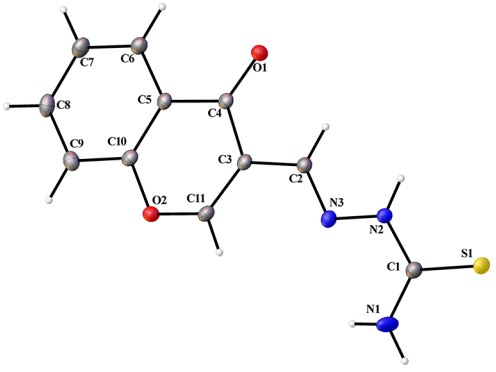

Figure 2. Molecular structure of SVSL1 showing the atomic labeling scheme and thermal ellipsoids at the 50% probability level.

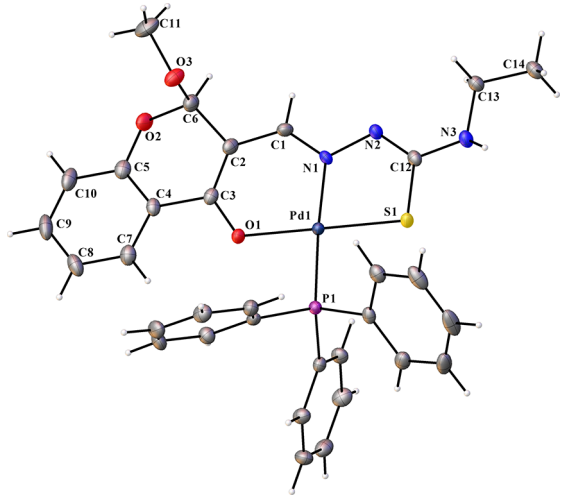

Figure 3. Molecular structure of **2** showing the atomic labeling scheme and thermal ellipsoids at the 50% probability level.

respectively. The structural parameters and data collection details for SVSL1 and complex **2** are provided in Table S2. Ligand SVSL1 crystallized in the primitive monoclinic $P2_1/c$ space group. Complex **2** crystallized in the monoclinic crystal system with the $P2_1/n$ space group. The complex adopted a distorted square planar geometry. The Pd(II) ion bound to O^-, N, and S^- donor atoms of the TSC ligand in such way that six- and five-membered rings were formed, and the fourth coordination site was occupied by triphenylphosphine. In the structure of complex **2**, increase in the C−O and C−S bond lengths and decrease in the C═N bond length were noted compared to those in the corresponding ligand.[71]

In addition, the methoxy group present in the C2 position of chromone moiety of the ligand clearly suggested the involvement of *in situ* Michael addition during the complex formation.[56,72] NMR and FT-IR spectra of the complexes also showed the same. It is expected that the ligand initially coordinates to the Pd(II) ion via azomethine nitrogen and thiolato sulfur (after enolization and deprotonation). Then methanol undergoes Michael addition at the C2 carbon of chromone to form the Michael adduct. Finally, anionic oxygen (after deprotonation of −OH) binds with the Pd(II) ion to

https://dx.doi.org/10.1021/acs.inorgchem.0c02373
Inorg. Chem. 2020, 59, 17109−17122

give the Pd(II) complex. Surprisingly, there is no precedence for such synthesis of Pd(II) complexes, that too under mild conditions. This might be a key scheme for developing new anticancer drugs and catalysts in the future. With the similar chromone TSC ligands containing a methyl or phenyl substituent at the terminal N, a different transformation was observed with Pd(II); however, this reaction was not carried out in an inert atmosphere.[56]

Spectroscopic Evidences for Michael Addition. An aliquot of the reaction mixture was taken immediately after the addition of Pd precursor $[PdCl_2(PPh_3)_2]$ to SVSL3, and analyzed. Peaks were seen at m/z 263.0990 $[PPh_3, M + H]^+$, 696.1099 $[\mathbf{3}, M - CH_3OH]^+$, and 728.1390 $[\mathbf{3}, M + H]^+$ in its mass spectrum. The reaction was allowed to proceed further for 10 min, and an aliquot was taken and analyzed after 5 and 10 min. No mass spectral changes were observed. The comparison of these spectra is illustrated in Figure S26. Moreover, ^1H NMR spectra taken for these aliquots and SVSL3 were compared (Figure S19). All the spectral results indicated that the formation of complex **3** took place via Michael addition in a very short time. Scheme 3 depicts the plausible mechanism for the formation of Pd(II) complexes from the corresponding ligands.

Scheme 3. Plausible Mechanism for the Formation of the Pd(II) Complexes

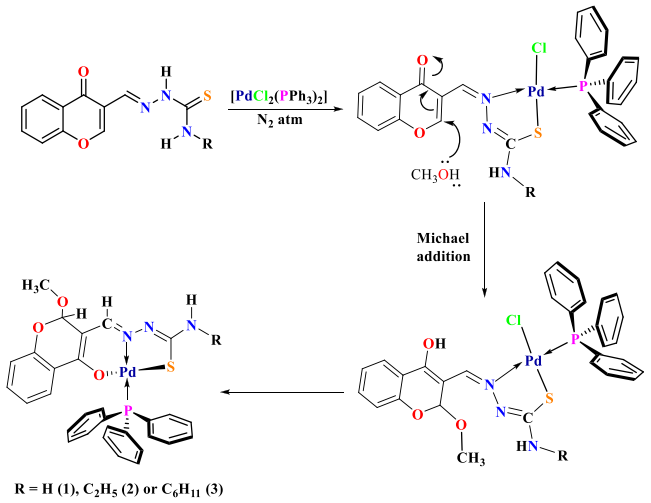

Stability in Water Medium. Stability of the complexes was tested in 1% DMSO−water mixture using UV−vis spectroscopy. There was almost negligible change in the spectra of the complexes, which indicated that the complexes were stable in water (Figure S27).

Intercalation with DNA. Anticancer agents are complexes known to show activity by binding to DNA either covalently or noncovalently. Noncovalent interactions occur through an intercalative, an electrostatic, or a groove (minor or major) mode of binding, while in covalent interactions, labile ligand of complexes is exchanged by the N donor atom of the nucleotide in the base pairs of DNA.[73] The intercalative mode of binding of the present complexes with CT DNA was confirmed by UV−vis absorption, emission, and viscosity techniques, and the order of binding strength was found to be **3** > **1** > **2**. Complex **3** showed greater binding than the other two complexes. This may be due to the presence of cyclohexyl group in complex **3** in addition to triphenylphosphine, which shows hydrophobic interactions with DNA.[55,73] The results and detailed discussion are provided in the Supporting Information (Figures S28−S30 and Table S3).

In addition to UV−vis, fluorescence, and viscosity studies, a thermal denaturation technique was used to confirm the intercalation mode of binding of the complexes with CT DNA. In general, a high ΔT_m value represents an intercalative mode of binding of a compound with DNA, while a low value (1−3 °C) refers to the groove and/or electrostatic binding mode(s). The thermal denaturation experiment carried out at a wavelength of 260 nm for CT DNA alone gave a T_m value of 61.0 °C (Figure S31). Upon addition of complexes **1**−**3**, the T_m value increased to 67.1 (±0.5)−68.2 (±1.5) °C. The ΔT_m (6.1−7.2 °C) values of CT DNA in the presence of the complexes were comparable to those observed for the classical intercalators, suggesting the significant DNA binding affinity of the complexes.[74]

Furthermore, to probe the binding of the complexes with DNA hexamer $d(CGATCG)_2$ (PDB ID: 1Z3F), MD studies were performed (Table S5). The intercalation mode of binding of the Pd(II) complexes with DNA is shown in Figure S32. As expected, complex **3** exhibited six hydrogen bonding interactions with DNA. A terminal N−H formed two hydrogen bonding interactions with the phosphate oxygen. The OCH_3 group formed two hydrogen bonding interactions with the NH_2 of DC-5, and the other oxygen atoms displayed hydrogen bonding interactions with the NH_2 of DC-1 and DG-2. In addition, cyclohexyl ring exhibited hydrophobic interactions with the backbone of DNA. The results of docking studies offered proof that the complexes bound to DNA via intercalation mode, which is in accordance with the experimental findings.[75,76]

Binding with Protein. The complexes quenched the inherent fluorescence of BSA protein due to their binding with BSA. Solving the Stern−Volmer and Scatchard equations using the plot of $F°/F$ versus [Q] gave the quenching constant (K_q) values [1.37×10^5 (**1**), 1.29×10^5 (**2**), and 2.24×10^5 (**3**)] which followed the order **3** > **1** > **2** (Figures S33−S35 and Table S4). Complex **3** was a better quencher than the other two complexes, which was due to the interactions of both triphenylphosphine and cyclohexyl groups with the active site amino acids of BSA. The possible interactions between complex **3** and BSA were investigated through MD studies.[52,55,77] UV−vis absorption spectra of BSA recorded in the presence of complexes **1**−**3** predicted a static type of quenching.[78] Upon incremental addition of the complexes to BSA, the fluorescence intensity of tyrosine residue ($\Delta\lambda$ = 15 nm) at 304 nm decreased in the magnitudes of 65.3 (**1**), 61.1 (**2**), and 75.4% (**3**), and that of tryptophan residue ($\Delta\lambda$ = 60 nm) at 345 nm decreased by 70.1, 69.5 and 78.6% for complexes **1**, **2**, and **3**, respectively (Figure S36 and S37). The results from synchronous spectral study suggested that all the complexes brought about changes in the microenvironment of both tyrosine and tryptophan residues, but more so in tryptophan than in tyrosine.[55]

Complex **3** showed the highest binding energy (−7.90 kcal/mol) among the three complexes docked with BSA (PDB ID: 3V03). The N−H group in complex **3** formed hydrogen bonding (2.3 Å) with C═O of ARG-208 (Figure S38 and Table S5). A polar interaction existed between heterocyclic oxygen and ASP-323 residue. The phenyl rings of triphenylphosphine exhibited hydrophobic interactions with VAL-215, PHE-227, THR-231, and ALA-324 amino acid residues, while

https://dx.doi.org/10.1021/acs.inorgchem.0c02373
Inorg. Chem. 2020, 59, 17109−17122

Table 1. IC_{50} (μM) Values of the Pd(II) Complexes and the Benchmark Compounds[84−87] in PANC-1, AsPC-1, MCF-7, MDA-MB-231, and MCF-10a Cells as Determined by MTT Assay after 72 h Incubations at 37°C[a]

	cancer cells				normal cells
	IC_{50} (μM)				IC_{50} (μM)
compound	PANC-1	AsPC-1	MCF-7	MDA-MB-231	MCF-10a
cisplatin	33.03 ± 0.04	19.01 ± 0.15	19.14 ± 0.17	7.1 ± 0.02	39.33 ± 1.14
carboplatin	36.08 ± 0.14	21.18 ± 0.02	22.7 ± 0.09	7.9 ± 0.14	41.05 ± 0.41
gemcitabine	21.8 ± 0.02	15.4 ± 0.14	5.85 ± 0.17	≥50	≥50
1	2.1 ± 0.02	4.9 ± 0.14	14.6 ± 0.23	1.52 ± 0.65	≥50
2	1.46 ± 0.02	1.35 ± 0.15	9.34 ± 0.11	0.7 ± 0.58	≥50
3	1.1 ± 0.02	0.9 ± 0.06	7.56 ± 0.42	0.5 ± 0.12	≥50

[a]Results are mean ± SD.

one of them also formed a π−cationic interaction with LYS-211. The cyclohexyl ring fit into the hydrophobic pocket that consisted of VAL-215, LEU-326, GLY-327, LEU-330, LEU-346, and GLU-353 amino acid residues.[79]

Cytotoxic to Cancer Cells. Cytotoxicity of the Pd(II) complexes was assessed against PANC-1, AsPC-1, MCF-7, and MDA-MB-231 cancer cell lines and MCF-10a cell line along with standard anticancer therapeutics, cisplatin, carboplatin, and gemcitabine (Table 1).

Interestingly, the Pd(II) complexes showed very good activity, and lower toxicity than the positive controls used in the normal cell line (MCF-10a). The cell viability was time-dependent, and the results confirmed the potent antiproliferative activity of the complexes against the tested cancer cell lines (Figures S39−S43). The complexes showed the IC_{50} values of 1.1−2.1 ± 0.02 μM in PANC-1 cancer cell line, which were 10 times lower than the ones observed for the standard drugs. The complexes showed higher IC_{50} values in MCF-7 (7.56 ± 0.42 to 1.52 ± 0.65 μM) and AsPC-1 (4.9 ± 0.14 to 0.9 ± 0.06 μM) cancer cell lines, but they were still lower than those exhibited by the positive controls. Superior activity of the complexes was seen in the MDA-MB-231 cell line, with the lowest IC_{50} value of 0.5 ± 0.12 μM exhibited by complex **3**. The higher activity of complex **3** can be attributed to the presence of a hydrophobic cyclohexyl substituent.[52] The IC_{50} values obtained for the present complexes are comparable to the ones obtained previously for the Pd(II) complexes incubated for 72 h.[80−83] The results proposed that the prepared Pd(II) complexes can be potential candidates for application in chemotherapy, given their selectivity toward cancer cells over normal cells.

Apoptotic Mode of Cell Death. Generally, healthy cells have spherical nuclei wherein the DNA is evenly distributed. During apoptosis, the natural mechanism adopted by living systems to eradicate damaged cells, the DNA undergoes condensation which can be detected via Hoechst staining.[88] Liu et al. reported that the various stages of apoptotic cells could be detected by AO/EB staining. A yellow-green AO nuclear stain marks the early stage apoptotic cells, whereas the late stage ones are marked by an asymmetric and localized orange nuclear EB stain.[89] In order to view these morphological changes induced by the complexes, MDA-MB-231 cancer cells were stained with Hoechst 33258 and AO/EB after treatment with the complexes for 48 h (Figures 4 and 5).

The apoptotic features such as nuclear swelling, cytoplasmic vacuolation, chromatin fragmentation, and cytoplasmic blebbing were observed.[3] Figuratively, the viable cells (control)

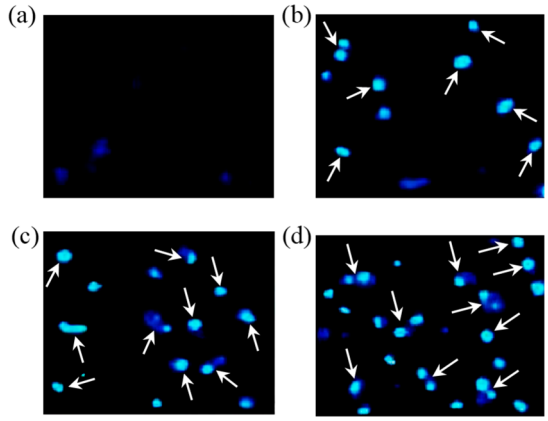

Figure 4. Hoechst 33258 staining of MDA-MB-231 cells for 48 h: control (a) and complexes **1** (b), **2** (c), and **3** (d).

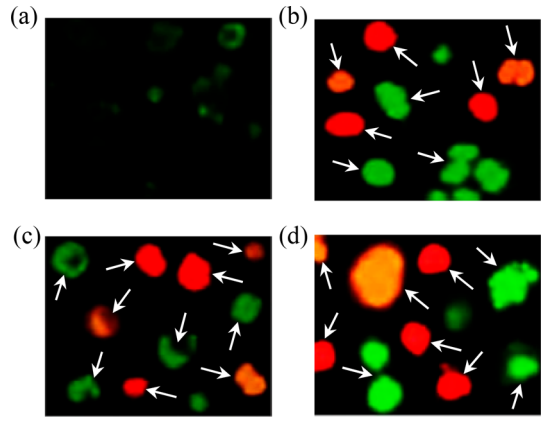

Figure 5. AO/EB staining of MDA-MB-231 cells for 48 h: control (a) and complexes **1** (b), **2** (c), and **3** (d).

contained green nuclei alongside an ordered structure, and early apoptotic cells contained green nuclei besides perinuclear chromatin condensation as bright green patches. Late apoptotic cells contained orange to red nuclei alongside condensed chromatin, and necrotic cells of homogeneously larger size contained orange to red nuclei without condensed chromatin.[90] Altogether, these morphological variations proposed that the complexes provoked cell death through apoptosis, and complex **3** displayed the highest apoptotic activity than the other two complexes in both the staining methods.

Nuclear Morphological Changes in MDA-MB-231. DAPI visualizes nuclear DNA in both the living and fixed

https://dx.doi.org/10.1021/acs.inorgchem.0c02373
Inorg. Chem. 2020, 59, 17109−17122

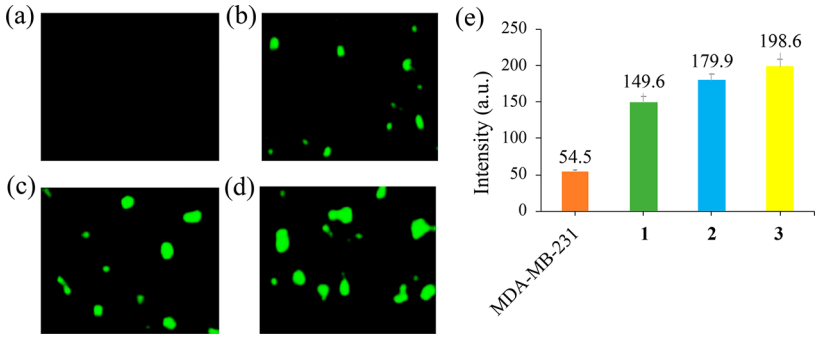

Figure 6. DCFH-DA stained MDA-MB-231 cells: control (a) and complexes **1** (b), **2** (c), and **3** (d). The fluorescence intensities of the complexes along with the control (e).

cells. DAPI staining is also used to determine the number of nuclei and assess gross cell morphology.[91] Prior to DAPI staining and observation under a fluorescence microscope, the complexes were treated with MDA-MB-231 cells for 48 h (Figure S44). The blue channel ($\lambda_{excitation}$ = 340 nm) showed the DAPI-stained nuclei, and the red channel ($\lambda_{excitation}$ = 456 nm) indicates the luminescence of the complexes. The overlay showed the total superimposition of the blue channel with the red channel, which indicated that the complexes induced nuclear damage and thus exposed the dispersed cytoplasmic and nuclear fluorescence.[68,92]

Reactive Oxygen Species (ROS) Generation. Numerous anticancer and chemotherapeutic agents stimulate apoptosis via ROS generation. DCFH-DA dye is one among the most extensively used tools for detecting ROS species. The dye is beneficial since it can permeate the cell and gets hydrolyzed to DCFH carboxylate anion intracellularly, which is retained by the cell. A fluorescent product, dichlorofluorescein (DCF), is formed as a result of $2e^-$ oxidation of DCFH due to the presence of intracellular ROS species, which then can be monitored.[93] The complexes were examined for their ROS generation ability using fluorescent probe DCFH-DA.[94] The complex-treated cells displayed an enhancement in the DCF fluorescence intensity. The fluorescence intensities were higher than that shown by the control (Figure 6). The fluorescence intensity of DCF was found to be 198.6 a.u. when MDA-MB-231 cells were treated with complex **3**, which is approximately 4 times more than that displayed by the cells treated with the control. The capability of complex **3** to display higher cytotoxicity than the other two complexes may be attributed to its ability to effectively generate ROS which promote apoptosis.[3,95]

Mitochondrial-Mediated Apoptosis. Western blotting technique enables us to identify selected proteins in a mixture of proteins that has been extracted from the cell. This helps in the monitoring of the cellular upregulation of certain proteins during an apoptotic cycle.[96] To elucidate the mechanism adopted by the complexes to bring about apoptosis, Western blot analysis was applied to the anti- and pro-apoptotic bodies of proteins as well as caspases (Figure 7).

There was a downregulation of anti-apoptotic protein and an upregulation of pro-apoptotic ones which were characteristics for the induction of intrinsic pathway of apoptosis. There was also an upregulation of caspase-3 and caspase-9, which were involved in the final step of caspase cascade triggering demise of the cell through apoptosis (Figure 8). Complex **3**, yet again showed a better activity, which lead to the conclusion that the complexes induced apoptosis through mitochondrial mediated pathway.

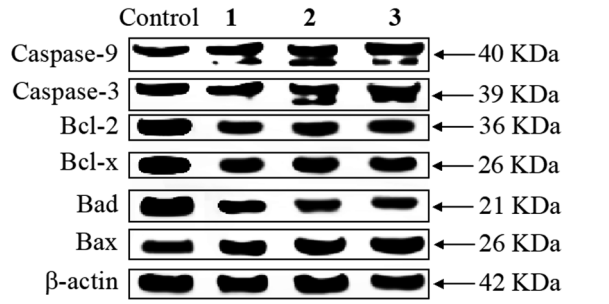

Figure 7. Western blot analysis of caspase-3, caspase-9, Bcl-2, Bcl-x, Bad, and Bax in MDA-MB-231 cells treated with complexes **1**, **2**, and **3** for 48 h. β-Actin was used as an internal control.

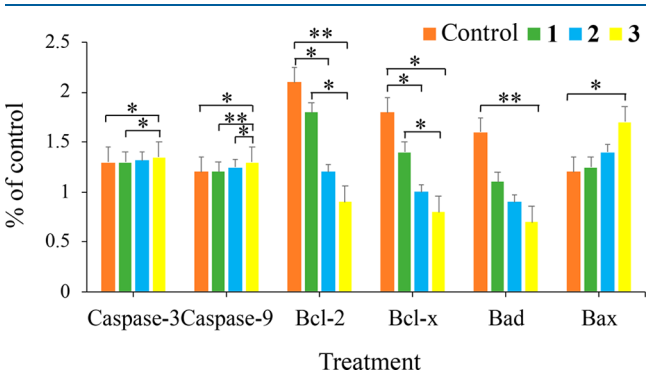

Figure 8. Percentage expression levels of caspase-3, caspase-9, Bcl-2, Bcl-x, Bad, and Bax in MDA-MB-231 cells treated with complexes **1**, **2**, and **3** for 48 h relative to the control (β-actin). Results are the mean ± SD (n = 6). *, $p < 0.05$; **, $p < 0.01$.

Cell Cycle Arrest. A cell cycle can be divided into four distinct phases: G1, S (DNA synthesis phase), G2, and M (mitosis). However, G2 and M phases have indistinguishable DNA content and hence could not be distinguished based on their dissimilarities in DNA content.[97] The cell viability assays exposed recognizable alterations in the cellular morphology that were consistent with apoptosis. Cell cycle analysis was carried out for the complexes in MDA-MB-231 cells to quantify the apoptotic cells (Figure 9). Propidium iodide (PI) is said to identify the dead cells which are apoptotic in the sub-G1 region of the cell cycle, although viable cell membranes are relatively impermeable to it. On treatment of MDA-MB-231 cells with the Pd(II) complexes at their IC_{50} concentration for

https://dx.doi.org/10.1021/acs.inorgchem.0c02373
Inorg. Chem. 2020, 59, 17109−17122

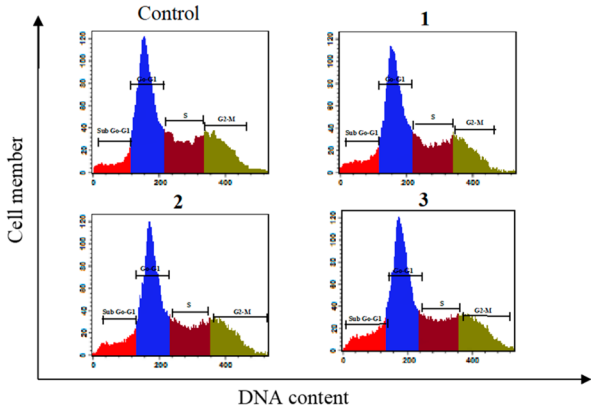

Figure 9. Cell cycle analysis of MDA-MB-231 cells treated with the IC_{50} concentration of complexes **1**, **2**, and **3** for 48 h.

48 h, the cell population in sub-G0/G1 phase increased from 1.21% (control) to 14.6, 23.5, and 34.5%, respectively, for complexes **1**−**3**, with slight changes in phases: G0/G1 (from 54.36% in the control to 53.23, 54.35, and 55.71%, respectively, for complexes **1**−**3**), S (from 24.5% in the control to 26.78, 25.93, and 23.2%, respectively, for complexes **1**−**3**), and G2/M (from 28.3% in the control to 31.2, 29.4, and 30.6%, respectively, for complexes **1**−**3**), indicating apoptosis induction. Over 50% cells were observed in the sub-G1 (apoptotic) region of the cell cycle (Figure 10).[74,98] This

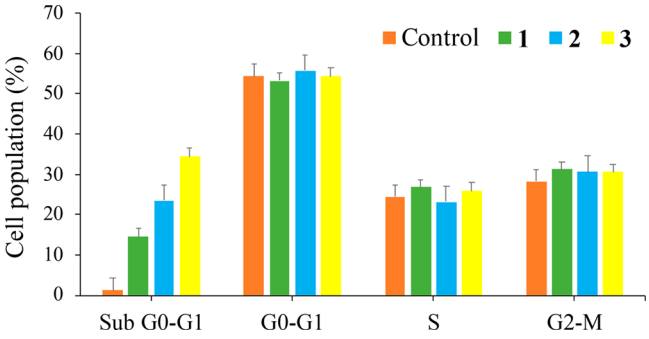

Figure 10. Percentage cell population in various phases of MDA-MB-231 cell cycle when treated with complexes **1**, **2**, and **3** for 48 h.

substantial number of cells in the sub-G1 population lead us to conclude that apoptosis was indeed the mechanism by which the Pd(II) complexes induced cell death. A possible cell death mechanism is shown in Figure 11.

Interaction with SARS-CoV-2 Main Protease and Other Receptors. Interactions at the active sites of VEGFR2 and EGFR are tabulated (Table S6) and represented in Figures S45−S46. The COVID-19 drug pipeline has not been propagated as much as the pandemic, but its rate of expansion is nevertheless cause for pause. Since the beginning of this year, there have been more than 180 clinical trials launched by researchers of everything from repurposed antivirals and immuno-modulators to unproven cell therapies and vitamin C.[99] To date, several metal complexes were reported to show good antiviral properties, and we have used an *in silico* MD method to identify the binding potential of Pd(II) complexes **1**−**3** with the SARS-CoV-2 main protease. The main protease is the best characterized drug target as this enzyme is highly essential in the replication of the virus. Docking energy, an indication of the ligand binding efficiency,

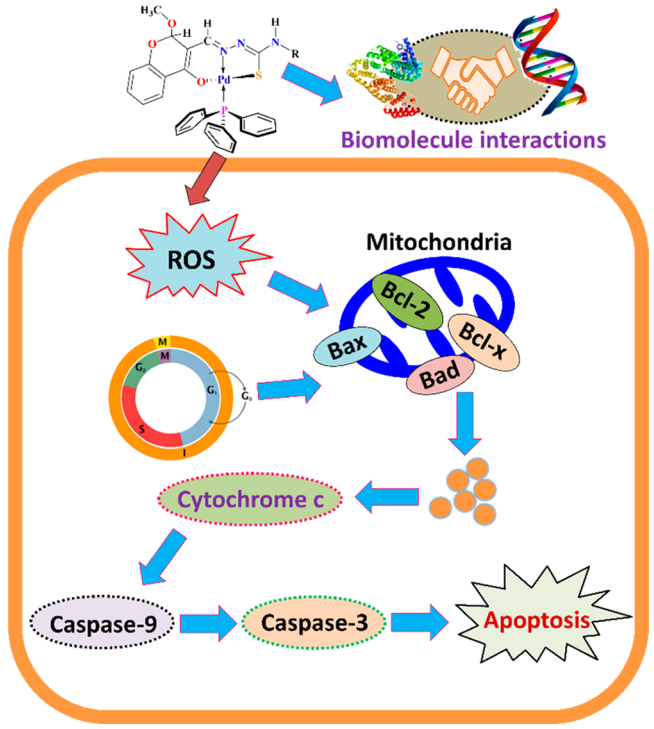

Figure 11. Proposed cell death mechanism for the Pd(II) complexes in MDA-MB-231 cancer cells.

of the enzyme−palladium complexes (−8.70, −8.39, and −9.38 kcal/mol for **1**, **2**, and **3**, respectively) was comparable with that of cocrystal ligand alpha-ketoamide (−8.41 kcal/mol) but much better than those of chloroquine (−5.60 kcal/mol) and hydroxychloroquine (−6.01 kcal/mol). Complex **3** showed good binding energy among the compounds used in the present study and had nonbonding interactions with active site residues THR-25, THR-26, HIS-41, CYS-44, MET-49, TYR-54, ASN-142, GLY-143, SER-144, CYS-145, HIS-163, GLU-166, ASP-187, and GLN-189. Interactions of cocrystal ligand, chloroquine, hydroxychloroquine, and complexes **1**−**3** at the active site of the enzyme are represented in Figure 12.

CONCLUSIONS

Three novel Pd(II) Michael adduct chromone TSC complexes (**1**−**3**) were synthesized and characterized. A distorted square planar geometry was proposed for the complexes. The synthetic route of the present complexes is novel and was proved by spectroscopic and single-crystal XRD tools. Complex **3** showed the highest binding efficacy toward CT DNA and BSA. Cytotoxicity of these complexes was evaluated against a panel of four human cancer cell lines (PANC-1, AsPC-1, MCF-7, and MDA-MB-231) and one normal (MCF-10a) cell line along with standard anticancer drugs (cisplatin, carboplatin, and gemcitabine). Complex **3** (IC_{50} = 0.5 μM) showed an exceptional activity in the MDA-MB-231 cell line wherein the IC_{50} value was nearly 7 or 50 times lower than that of cisplatin (IC_{50} = 7.1 μM), carboplatin (IC_{50} = 7.9 μM), or gemcitabine (IC_{50} ≥ 50). The same complex exhibited potential activity against PANC-1 and AsPC-1 cells with IC_{50} values of 1.1 and 0.9 μM, respectively. Cytotoxicity results of the complexes were compared with those of cisplatin, carboplatin, and gemcitabine, and it was inferred that all the complexes exhibited higher activity than the standard drugs.

https://dx.doi.org/10.1021/acs.inorgchem.0c02373
Inorg. Chem. 2020, 59, 17109−17122

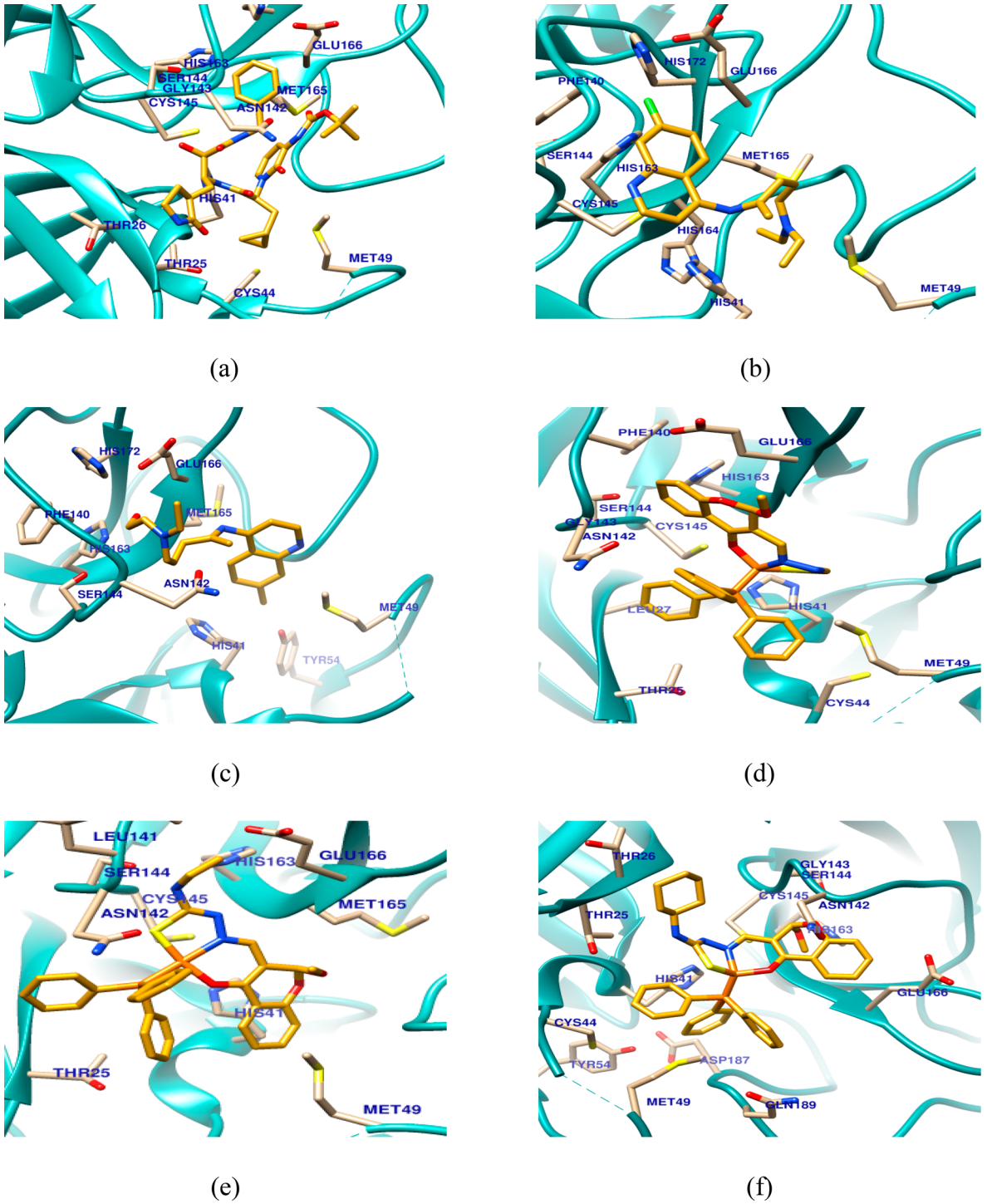

Figure 12. Binding mode of cocrystal ligand alpha-ketoamide (a), chloroquine (b), hydroxychloroquine (c), **1** (d), **2** (e), and **3** (f) at the active site of SARS-CoV-2 main protease.

Furthermore, to elucidate the inhibition mechanism of the complexes, staining assays were employed. Hoechst, AO/EB, and DAPI staining imparted that besides cellular uptake of the complexes, there were apoptotic like morphological changes happening in MDA-MB-231 cancer cells. Additionally, DCFH-DA staining assay revealed the generation of ROS species in the cancer cells. Along with the results obtained from cell cycle arrest and Western blot analysis, it was confirmed that the complexes induced cell death through the intrinsic pathway of apoptosis. The complexes showed good *in silico* binding energies with VEGFR2, EGFR, and the SARS-CoV-2 main protease. The docking energies of the SARS-CoV-2 main protease with the Pd complexes (−8.70, −8.39, and −9.38 kcal/mol for **1**, **2**, and **3** respectively) were comparable with that of cocrystal ligand (−8.41 kcal/mol) and much better than those of chloroquine (−5.60 kcal/mol) and hydroxychloroquine (−6.01 kcal/mol). *In vitro* studies will be carried out for these complexes to establish their usefulness as clinical antiviral agents.

https://dx.doi.org/10.1021/acs.inorgchem.0c02373
Inorg. Chem. 2020, 59, 17109−17122

■ ASSOCIATED CONTENT

Supporting Information

The Supporting Information is available free of charge at https://pubs.acs.org/doi/10.1021/acs.inorgchem.0c02373.

Experimental procedures for biomolecular interactions and antiproliferative studies, results of DNA/BSA binding and molecular docking with the targeted proteins, NMR spectra of the compounds (PDF)

Accession Codes

CCDC 2000214−2000215 contain the supplementary crystallographic data for this paper. These data can be obtained free of charge via www.ccdc.cam.ac.uk/data_request/cif, or by emailing data_request@ccdc.cam.ac.uk, or by contacting The Cambridge Crystallographic Data Centre, 12 Union Road, Cambridge CB2 1EZ, UK; fax: +44 1223 336033.

■ AUTHOR INFORMATION

Corresponding Author

Ramasamy Karvembu − *Department of Chemistry, National Institute of Technology, Tiruchirappalli 620015, India;* orcid.org/0000-0001-8966-8602; Email: kar@nitt.edu

Authors

Jebiti Haribabu − *Department of Chemistry, National Institute of Technology, Tiruchirappalli 620015, India*

Swaminathan Srividya − *Department of Chemistry, National Institute of Technology, Tiruchirappalli 620015, India*

Dharmasivam Mahendiran − *Department of Pathology, Bosch Institute, University of Sydney, Sydney, New South Wales 2006, Australia*

Dasararaju Gayathri − *Centre of Advanced Study in Crystallography and Biophysics, University of Madras, Guindy Campus, Chennai 600025, India*

Vemula Venkatramu − *Department of Physics, Krishna University Dr. MRAR PG Centre, Nuzvid 521201, India*

Nattamai Bhuvanesh − *Department of Chemistry, Texas A & M University, College Station, Texas 77842, United States*

Complete contact information is available at: https://pubs.acs.org/10.1021/acs.inorgchem.0c02373

Author Contributions

#S.S. and D.M. contributed equally to this work.

Notes

The authors declare no competing financial interest.

■ ACKNOWLEDGMENTS

R.K. thanks SERB for the financial support. S.S. thanks the Department of Science and Technology, Ministry of Science and Technology, Government of India, for a doctoral fellowship under the DST-INSPIRE (IF160449) program. We are thankful to Dr. Sodio C. N. Hsu, Department of Medicinal and Applied Chemistry, Kaohsiung Medical University, Kaohsiung 807, Taiwan, for mass analysis.

■ REFERENCES

(1) Iqbal, P. F.; Malik, M. A.; Wani, W. A. Serendipity of cisplatin, and the emergence of metallodrugs in cancer chemotherapy. *World J. Pharm. Pharm. Sci.* **2018**, *7*, 654−664.

(2) Czajkowska-Szczykowska, D.; Morzycki, J. W.; Wojtkielewicz, A. Pd-catalyzed steroid reactions. *Steroids* **2015**, *97*, 13−44.

(3) Swaminathan, S.; Haribabu, J.; Kalagatur, N. K.; Konakanchi, R.; Balakrishnan, N.; Bhuvanesh, N.; Karvembu, R. Synthesis and anticancer activity of $[RuCl_2(\eta^6\text{-arene})(aroylthiourea)]$ complexes - High activity against the human neuroblastoma (IMR-32) cancer cell line. *ACS Omega* **2019**, *4*, 6245−6256.

(4) Allardyce, C. S.; Dyson, P. J. Metal-based drugs that break the rules. *Dalton Trans.* **2016**, *45*, 3201−3209.

(5) Padhye, S.; Afrasiabi, Z.; Sinn, E.; Fok, J.; Mehta, K.; Rath, N. Antitumor metallothiosemicarbazonates: Structure and antitumor activity of palladium complex of phenanthrenequinone thiosemicarbazone. *Inorg. Chem.* **2005**, *44*, 1154−1156.

(6) Bharti, N.; Athar, F.; Maurya, M. R.; Azam, A. Synthesis, characterization and *in vitro* anti-amoebic activity of new palladium(II) complexes with 5-nitrothiophene-2-carboxaldehyde N(4)-substituted thiosemicarbazones. *Bioorg. Med. Chem.* **2004**, *12*, 4679−4684.

(7) Ruiz, J.; Cutillas, N.; Vicente, C.; Villa, M. D.; López, G.; Lorenzo, J.; Avilés, F. X.; Moreno, V.; Bautista, D. New palladium(II) and platinum(II) complexes with the model nucleobase 1-methylcytosine: Antitumor activity and interactions with DNA. *Inorg. Chem.* **2005**, *44*, 7365−7376.

(8) Graham, R. D.; Williams, D. R. The synthesis and screening for anti-bacterial, -cancer, -fungicidal and -viral activities of some complexes of palladium and nickel. *J. Inorg. Nucl. Chem.* **1979**, *41*, 1245−1249.

(9) Gavrish, S. P.; Lampeka, Y. D.; Babak, M. V.; Arion, V. B. Palladium complexes of N,N′-bis(2-aminoethyl)oxamide (H_2L): Structural ($Pd^{II}L$, $Pd^{II}_2L_2$, and $Pd^{IV}LCl_2$), electrochemical, dynamic ^1H NMR and cytotoxicity studies. *Inorg. Chem.* **2018**, *57*, 1288−1297.

(10) Kapdi, A. R.; Fairlamb, I. J. S. Anti-cancer palladium complexes: A focus on PdX_2L_2, palladacycles and related complexes. *Chem. Soc. Rev.* **2014**, *43*, 4751−4777.

(11) Kalaiarasi, G.; Dharani, S.; Lynch, V. M.; Prabhakaran, R. *Para* metallation of 3-acetyl-chromen-2-one Schiff bases in tetranuclear palladacycles: Focus on their biomolecular interaction and *in vitro* cytotoxicity. *Dalton Trans.* **2019**, *48*, 12496−12511.

(12) Cullinane, C.; Deacon, G. B.; Drago, P. R.; Erven, A. P.; Junk, P. C.; Luu, J.; Meyer, G.; Schmitz, S.; Ott, I.; Schur, J.; Webster, L. K.; Klein, A. Synthesis and antiproliferative activity of a series of new platinum and palladium diphosphane complexes. *Dalton Trans.* **2018**, *47*, 1918−1932.

(13) Quiroga, A. G.; Ranninger, C. N. Contribution to the SAR field of metallated and coordination complexes. Studies of the palladium and platinum derivatives with selected thiosemicarbazones as antitumoral drugs. *Coord. Chem. Rev.* **2004**, *248*, 119−133.

(14) Shao, J.; Bao, W.-G.; Tian, H.; Li, B.; Zhao, X.-F.; Qiao, X.; Xu, J.-Y. Nuclease activity and protein-binding properties of a novel tetranuclear thiosemicarbazide Pt(II) complex. *Dalton Trans.* **2014**, *43*, 1663−1671.

(15) Vojtek, M.; Marques, M. P. M.; Ferreira, I. M. P. L. V. O.; Mota-Filipe, H.; Diniz, C. Anticancer activity of palladium-based complexes against triple-negative breast cancer. *Drug Discovery Today* **2019**, *24*, 1044−1058.

(16) West, D. X.; Liberta, A. E.; Padhye, S. B.; Chikate, R. C.; Sonawane, P. B.; Kumbhar, A. S.; Yerande, R. G. Thiosemicarbazone complexes of copper(II): Structural and biological studies. *Coord. Chem. Rev.* **1993**, *123*, 49−71.

(17) Casas, J.; García-Tasende, M.; Sordo, J. Main group metal complexes of semicarbazones and thiosemicarbazones: A structural review. *Coord. Chem. Rev.* **2000**, *209*, 197−261.

(18) Kovacevic, Z.; Menezes, S. V.; Sahni, S.; Kalinowski, D. S.; Bae, D. H.; Lane, D. J. R.; Richardson, D. R. The metastasis suppressor, N-MYC downstream-regulated gene-1 (NDRG1), down-regulates the ErbB family of receptors to inhibit downstream oncogenic signaling pathways. *J. Biol. Chem.* **2016**, *291*, 1029−1052.

(19) Ibrahim, A. A.; Khaledi, H.; Hassandarvish, P.; Mohd Ali, H.; Karimian, H. Indole-7-carbaldehyde thiosemicarbazone as a flexidentate ligand toward Zn^{II}, Cd^{II}, Pd^{II} and Pt^{II} ions: Cytotoxic and apoptosis-inducing properties of the Pt^{II} complex. *Dalton Trans.* **2014**, *43*, 3850−3860.

(20) Saswati, S.; Chakraborty, A.; Dash, S. P.; Panda, A. K.; Acharyya, R.; Biswas, A.; Mukhopadhyay, S.; Bhutia, S. K.; Crochet, A.; Patil, Y. P.; et al. Synthesis, X-ray structure and *in vitro* cytotoxicity studies of Cu(I/II) complexes of thiosemicarbazone: Special emphasis on their interactions with DNA. *Dalton Trans.* **2015**, *44*, 6140−6157.
(21) Wang, B.; Yang, Z.-Y.; Lü, M.; Hai, J.; Wang, Q.; Chen, Z.-N. Synthesis, characterization, cytotoxic activity and DNA binding of Ni(II) complex with the 6-hydroxy chromone-3-carbaldehyde thiosemicarbazone. *J. Organomet. Chem.* **2009**, *694*, 4069−4075.
(22) Genova, P.; Varadinova, T.; Matesanz, A. I.; Marinova, D.; Souza, P. Toxic effects of *bis*(thiosemicarbazone) compounds and its palladium(II) complexes on herpes simplex virus growth. *Toxicol. Appl. Pharmacol.* **2004**, *197*, 107−112.
(23) Matesanz, A. I.; Pérez, J. M.; Navarro, P.; Moreno, J. M.; Colacio, E.; Souza, P. Synthesis and characterization of novel palladium(II) complexes of *bis*(thiosemicarbazone): Structure, cytotoxic activity and DNA binding of Pd(II)-benzyl *bis*(thiosemicarbazonate). *J. Inorg. Biochem.* **1999**, *76*, 29−37.
(24) Kovala-Demertzi, D.; Demertzis, M. A.; Miller, J. R.; Papadopoulou, C.; Dodorou, C.; Filousis, G. Platinum(II) complexes with 2-acetyl pyridine thiosemicarbazone: Synthesis, crystal structure, spectral properties, antimicrobial and antitumour activity. *J. Inorg. Biochem.* **2001**, *86*, 555−563.
(25) Anjum, R.; Palanimuthu, D.; Kalinowski, D. S.; Lewis, W.; Park, K. C.; Kovacevic, Z.; Khan, I. U.; Richardson, D. R. Synthesis, characterization, and *in vitro* anticancer activity of copper and zinc *bis*(thiosemicarbazone) complexes. *Inorg. Chem.* **2019**, *58*, 13709−13723.
(26) Carcelli, M.; Tegoni, M.; Bartoli, J.; Marzano, C.; Pelosi, G.; Salvalaio, M.; Rogolino, D.; Gandin, V. *In vitro* and *in vivo* anticancer activity of tridentate thiosemicarbazone copper complexes: Unravelling an unexplored pharmacological target. *Eur. J. Med. Chem.* **2020**, *194*, 112266.
(27) Cao, W.; Qi, J.; Qian, K.; Tian, L.; Cheng, Z.; Wang, Y. Structure-activity relationships of 2-quinolinecarboxaldehyde thiosemicarbazone gallium(III) complexes with potent and selective anticancer activity. *J. Inorg. Biochem.* **2019**, *191*, 174−182.
(28) Marcaccini, S.; Neo, A. G.; Marcos, C. F. Sequential five-component synthesis of spiropyrrolidinochromanones. *J. Org. Chem.* **2009**, *74*, 6888−6890.
(29) Dziewulska-Kułaczkowska, A.; Mazur, L. Structural studies and characterization of 3-formylchromone and products of its reactions with chosen primary aromatic amines. *J. Mol. Struct.* **2011**, *985*, 233−242.
(30) Kanagalakshmi, K.; Premanathan, M.; Priyanka, R.; Hemalatha, B.; Vanangamudi, A. Synthesis, anticancer and antioxidant activities of 7-methoxyisoflavanone and 2,3-diarylchromanones. *Eur. J. Med. Chem.* **2010**, *45*, 2447−2452.
(31) Mayuri, B.; Kavitha, P.; Basavoju, S.; Bhargavi, G.; Reddy, K. L. Synthesis, structural characterisation and biological evolution of chromanones. *J. Mol. Struct.* **2017**, *1145*, 1−9.
(32) Meng, L.-G.; Liu, H.-F.; Wei, J.-L.; Gong, S.-N.; Xue, S. One-pot reaction of *ortho*-acylphenols and terminal alkynoates for synthesis of 2-alkyl-substituted chromanones. *Tetrahedron Lett.* **2010**, *51*, 1748−1750.
(33) Budzisz, E. Synthesis, reactions and biological activity of phosphorus-containing derivatives of chromone and coumarin. *Phosphorus, Sulfur Silicon Relat. Elem.* **2004**, *179*, 2131−2147.
(34) Hodgetts, K. J.; Maragkou, K. I.; Wallace, T. W.; Wootton, R. C. R. Conjugate addition to 3-arylsulfinylchromones as a synthetic route to homochiral 2-substituted chromanones: Scope and limitations. *Tetrahedron* **2001**, *57*, 6793−6804.
(35) Arjunan, V.; Subramanian, S.; Mohan, S. FTIR and FTR spectral studies of 2-amino-6-bromo-3-formylchromone. *Spectrochim. Acta, Part A* **2004**, *60*, 995−1000.
(36) Ishar, M. P. S.; Singh, G.; Singh, S.; Sreenivasan, K. K.; Singh, G. Design, synthesis, and evaluation of novel 6-chloro/fluorochromone derivatives as potential topoisomerase inhibitor anticancer agents. *Bioorg. Med. Chem. Lett.* **2006**, *16*, 1366−1370.
(37) Dyck, B.; Zhao, L.; Tamiya, J.; Pontillo, J.; Hudson, S.; Ching, B.; Heise, C. E.; Wen, J.; Norton, C.; Madan, A.; Schwarz, D.; Wade, W.; Goodfellow, V. S. Substituted chromones and quinolones as potent melanin-concentrating hormone receptor 1 antagonists. *Bioorg. Med. Chem. Lett.* **2006**, *16*, 4237−4242.
(38) Sosnovskikh, V. Y.; Irgashev, R. A. Uncatalyzed addition of indoles and N-methylpyrrole to 3-formylchromones: Synthesis of (chromon-3-yl)bis(indol-3-yl)methanes and *E*-2-hydroxy-3-(1-methylpyrrol-2-ylmethylene)chroman-4-ones under solvent-free conditions. *Tetrahedron Lett.* **2007**, *48*, 7436−7439.
(39) Wang, B.; Yang, Z.-Y.; Qin, D.; Chen, Z.-N. Synthesis, characterization, cytotoxic activity and DNA binding properties of the Ln(III) complexes with ethylenediiminobi(6-hydroxychromone-3-carbaldehyde) Schiff base. *J. Photochem. Photobiol., A* **2008**, *194*, 49−58.
(40) Gaber, M.; El-Baradie, K.; El-Wakiel, N.; Hafez, S. Synthesis and characterization of 3-formyl chromone Schiff base complexes and their application as antitumor, antioxidant and antimicrobial. *Appl. Organomet. Chem.* **2020**, *34*, e5348.
(41) Nawrot-Modranka, J.; Nawrot, E.; Graczyk, J. *In vivo* antitumor, *in vitro* antibacterial activity and alkylating properties of phosphorohydrazine derivatives of coumarin and chromone. *Eur. J. Med. Chem.* **2006**, *41*, 1301−1309.
(42) Singh, G.; Singh, R.; Girdhar, N. K.; Ishar, M. P. S. A versatile route to 2-alkyl-/aryl-amino-3-formyl- and hetero-annelated-chromones, through a facile nucleophilic substitution at C2 in 2-(N-methylanilino)-3-formylchromones. *Tetrahedron* **2002**, *58*, 2471−2480.
(43) Sun, W.; Carroll, P. J.; Soprano, D. R.; Canney, D. J. Identification of a chromone-based retinoid containing a polyolefinic side chain *via* facile synthetic routes. *Bioorg. Med. Chem. Lett.* **2009**, *19*, 4339−4342.
(44) Jo, H.; Hee Seo, S.; Na, Y.; Kwon, Y. The synthesis and anticancer activities of chiral epoxy-substituted chromone analogs. *Bioorg. Chem.* **2019**, *84*, 347−354.
(45) Haribabu, J.; Jeyalakshmi, K.; Arun, Y.; Bhuvanesh, N. S. P.; Perumal, P. T.; Karvembu, R. Synthesis, DNA/protein binding, molecular docking, DNA cleavage and *in vitro* anticancer activity of nickel(II) bis(thiosemicarbazone) complexes. *RSC Adv.* **2015**, *5*, 46031−46049.
(46) Muralisankar, M.; Basheer, S. M.; Haribabu, J.; Bhuvanesh, N. S. P.; Karvembu, R.; Sreekanth, A. An investigation on the DNA/protein binding, DNA cleavage and *in vitro* anticancer properties of SNO pincer type palladium(II) complexes with N-substituted isatin thiosemicarbazone ligands. *Inorg. Chim. Acta* **2017**, *466*, 61−70.
(47) Muralisankar, M.; Haribabu, J.; Bhuvanesh, N. S. P.; Karvembu, R.; Sreekanth, A. Synthesis, X-ray crystal structure, DNA/protein binding, DNA cleavage and cytotoxicity studies of N(4)-substituted thiosemicarbazone based copper(II)/nickel(II) complexes. *Inorg. Chim. Acta* **2016**, *449*, 82−95.
(48) Rahman, K. N. A.; Haribabu, J.; Balachandran, C.; Bhuvanesh, N. S. P.; Karvembu, R.; Sreekanth, A. Copper, nickel and zinc complexes of 3-acetyl coumarin thiosemicarbazone: Synthesis, characterization and *in vitro* evaluation of cytotoxicity and DNA/protein binding properties. *Polyhedron* **2017**, *135*, 26−35.
(49) Haribabu, J.; Sabapathi, G.; Tamizh, M. M.; Balachandran, C.; Bhuvanesh, N. S. P.; Venuvanalingam, P.; Karvembu, R. Water-soluble mono- and bi-nuclear Ru(η^6-*p*-cymene) complexes containing indole thiosemicarbazones: Synthesis, DFT modelling, biomolecular interactions, and *in vitro* anticancer activity through apoptosis. *Organometallics* **2018**, *37*, 1242−1257.
(50) Haribabu, J.; Subhashree, G. R.; Saranya, S.; Gomathi, K.; Karvembu, R.; Gayathri, D. Synthesis, crystal structure, and *in vitro* and *in silico* molecular docking of novel acyl thiourea derivatives. *J. Mol. Struct.* **2015**, *1094*, 281−291.
(51) Haribabu, J.; Ranade, D. S.; Bhuvanesh, N. S. P.; Kulkarni, P. P.; Karvembu, R. Ru(II)-*p*-cymene thiosemicarbazone complexes as inhibitors of amyloid β (aβ) peptide aggregation and aβ-induced cytotoxicity. *Chemistry Select* **2017**, *2*, 11638−11644.

https://dx.doi.org/10.1021/acs.inorgchem.0c02373
Inorg. Chem. 2020, 59, 17109−17122

(52) Balakrishnan, N.; Haribabu, J.; Anantha Krishnan, D.; Swaminathan, S.; Mahendiran, D.; Bhuvanesh, N. S.P.; Karvembu, R. Zinc(II) complexes of indole thiosemicarbazones: DNA/protein binding, molecular docking and *in vitro* cytotoxicity studies. *Polyhedron* **2019**, *170*, 188−201.
(53) Balachandran, C.; Haribabu, J.; Jeyalakshmi, K.; Bhuvanesh, N. S. P.; Karvembu, R.; Emi, N.; Awale, S. Nickel(II) *bis*(isatin thiosemicarbazone) complexes induced apoptosis through mitochondrial signaling pathway and G0/G1 cell cycle arrest in IM-9 cells. *J. Inorg. Biochem.* **2018**, *182*, 208−221.
(54) Haribabu, J.; Jeyalakshmi, K.; Arun, Y.; Bhuvanesh, N. S. P.; Perumal, P. T.; Karvembu, R. Synthesis of Ni(II) complexes bearing indole-based thiosemicarbazone ligands for interaction with biomolecules and some biological applications. *JBIC, J. Biol. Inorg. Chem.* **2017**, *22*, 461−480.
(55) Haribabu, J.; Tamizh, M. M.; Balachandran, C.; Arun, Y.; Bhuvanesh, N. S. P.; Endo, A.; Karvembu, R. Synthesis, structures and mechanistic pathways of anticancer activity of palladium(II) complexes with indole-3-carbaldehyde thiosemicarbazones. *New J. Chem.* **2018**, *42*, 10818−10832.
(56) Haribabu, J.; Balachandran, C.; Tamizh, M. M.; Arun, Y.; Bhuvanesh, N. S. P.; Aoki, S.; Karvembu, R. Unprecedented formation of palladium(II)-pyrazole based thiourea from chromone thiosemicarbazone and $[PdCl_2(PPh_3)_2]$: Interaction with biomolecules and apoptosis through mitochondrial signalling pathway. *J. Inorg. Biochem.* **2020**, *205*, 110988.
(57) Remuzzi, A.; Remuzzi, G. COVID-19 and Italy: What next? *Lancet* **2020**, *395*, 1225−1228.
(58) *APEX2, Program for Data Collection and Integration on Area Detectors*; Bruker AXS Inc.: Madison, WI, 2016.
(59) (a) Sheldrick, G. M. A short history of SHELX. *Acta Crystallogr., Sect. A: Found. Crystallogr.* **2008**, *A64*, 112−122. (b) Sheldrick, G. M. SHELXT - Integrated space-group and crystal-structure determination. *Acta Crystallogr., Sect. A: Found. Adv.* **2015**, *A71*, 3−8. (c) Sheldrick, G. M. Crystal structure refinement with SHELXL. *Acta Crystallogr., Sect. C: Struct. Chem.* **2015**, *C71*, 3−8.
(60) Dolomanov, O. V.; Bourhis, L. J.; Gildea, R. J.; Howard, J. A. K.; Puschmann, H. Olex2: A complete structure solution, refinement and analysis program. *J. Appl. Crystallogr.* **2009**, *42*, 339−341.
(61) Jeyalakshmi, K.; Haribabu, J.; Balachandran, C.; Swaminathan, S.; Bhuvanesh, N. S. P.; Karvembu, R. Coordination behavior of N,N′,N″-trisubstituted guanidine ligands in their Ru-arene complexes: Synthetic, DNA/protein binding and cytotoxic studies. *Organometallics* **2019**, *38*, 753−770.
(62) Morris, G. M.; Huey, R.; Lindstrom, W.; Sanner, M. F.; Belew, R. K.; Goodsell, D. S.; Olson, A. J. AutoDock4 and AutoDockTools4: Automated docking with selective receptor flexibility. *J. Comput. Chem.* **2009**, *30*, 2785−2791.
(63) Canals, A.; Purciolas, M.; Aymami, J.; Coll, M. The anticancer agent ellipticine unwinds DNA by intercalative binding in an orientation parallel to base pairs. *Acta Crystallogr. Sect. Acta Crystallogr., Sect. D: Biol. Crystallogr.* **2005**, *61*, 1009−1012.
(64) Majorek, K. A.; Porebski, P. J.; Dayal, A.; Zimmerman, M. D.; Jablonska, K.; Stewart, A. J.; Chruszcz, M.; Minor, W. Structural and immunologic characterization of bovine, horse, and rabbit serum albumins. *Mol. Immunol.* **2012**, *52*, 174−182.
(65) Zhang, L.; Lin, D.; Sun, X.; Curth, U.; Drosten, C.; Sauerhering, L.; Becker, S.; Rox, K.; Hilgenfeld, R. Crystal structure of SARS-CoV-2 main protease provides a basis for design of improved α-ketoamide inhibitors. *Science* **2020**, *368*, 409−412.
(66) Berman, H. M.; Westbrook, J.; Feng, Z.; Gilliland, G.; Bhat, T. N.; Weissig, H.; Shindyalov, I. N.; Bourne, P. E. The protein data bank. *Nucleic Acids Res.* **2000**, *28*, 235−242.
(67) *Maestro*,version 8.5; Schrödinger, LLC: New York, 2008.
(68) Mahendiran, D.; Kumar, R. S.; Rahiman, A. K. Heteroleptic silver(I) complexes with 2,2′:6′,2″-terpyridines and naproxen: DNA interaction, EGFR/VEGFR2 kinase, growth inhibition and cell cycle arrest studies. *Mater. Sci. Eng., C* **2017**, *76*, 601−615.
(69) Bharathi, S.; Mahendiran, D.; Kumar, R. S.; Kim, Y. G.; Gajendiran, M.; Kim, K.; Rahiman, A. K. Biocompatibility, *in vitro* antiproliferative, and *in silico* EGFR/VEGFR2 studies of heteroleptic metal(II) complexes of thiosemicarbazones and naproxen. *Chem. Res. Toxicol.* **2019**, *32*, 1554−1571.
(70) Shanmugapriya, A.; Jain, R.; Sabarinathan, D.; Kalaiarasi, G.; Dallemer, F.; Prabhakaran, R. Structurally different mono-, bi- and trinuclear Pd(II) complexes and their DNA/protein interaction, DNA cleavage, and anti-oxidant, anti-microbial and cytotoxic studies. *New J. Chem.* **2017**, *41*, 10324−10338.
(71) Gangadharan, R.; Haribabu, J.; Karvembu, R.; Sethusankar, K. Crystal structures of two hydrazinecarbothioamide derivatives: (*E*)-N-ethyl-2-[(4-oxo-4H-chromen-3-yl) methylidene] hydrazinecarbothioamide hemi-hydrate and (*E*)-2-[(4-chloro-2H-chromen-3-yl)-methylidene]-N-phenylhydrazinecarbothioamide. *Acta Crystallogr., Sect. E: Crystallogr. Commun.* **2015**, *71*, 305−308.
(72) Zhao, L.; Xie, F.; Cheng, G.; Hu, Y. A base-promoted tandem reaction of 3-(1-alkynyl)chromones with 1,3-dicarbonyl compounds: An efficient approach to functional xanthones. *Angew. Chem., Int. Ed.* **2009**, *48*, 6520−6523.
(73) Huang, Y.-C.; Haribabu, J.; Chien, C.-M.; Sabapathi, G.; Chou, C.-K.; Karvembu, R.; Venuvanalingam, P.; Ching, W.-M.; Tsai, M.-L.; Hsu, S. C. N. Half-sandwich Ru(η^6-*p*-cymene) complexes featuring pyrazole appended ligands: Synthesis, DNA binding and *in vitro* cytotoxicity. *J. Inorg. Biochem.* **2019**, *194*, 74−84.
(74) Mahendiran, D.; Kumar, R. S.; Viswanathan, V.; Velmurugan, D.; Rahiman, A. K. Targeting of DNA molecules, BSA/c-Met tyrosine kinase receptors and antiproliferative activity of bis(terpyridine)-copper(II) complexes. *Dalton Trans.* **2016**, *45*, 7794−7814.
(75) Muralisankar, M.; Sujith, S.; Bhuvanesh, N. S. P.; Sreekanth, A. Synthesis and crystal structure of new monometallic and bimetallic copper(II) complexes with N-substituted isatin thiosemicarbazone ligands: Effects of the complexes on DNA/protein binding property, DNA cleavage study and *in vitro* anticancer activity. *Polyhedron* **2016**, *118*, 103−117.
(76) Ali, A.; Kamra, M.; Roy, S.; Muniyappa, K.; Bhattacharya, S. Enhanced G-quadruplex DNA stabilization and telomerase inhibition by novel fluorescein derived salen and salphen based Ni(II) and Pd(II) complexes. *Bioconjugate Chem.* **2017**, *28*, 341−352.
(77) Petrovic, A.; Zivanovic, M.; Puchta, R.; Cocic, D.; Scheurer, A.; Milivojevic, N.; Bogojeski, J. Experimental and quantum chemical study on the DNA/protein binding and the biological activity of a rhodium(III) complex with 1,2,4-triazole as an inert ligand. *Dalton Trans.* **2020**, *49*, 9070−9085.
(78) Jeyalakshmi, K.; Arun, Y.; Bhuvanesh, N. S. P.; Perumal, P. T.; Sreekanth, A.; Karvembu, R. DNA/protein binding, DNA cleavage, cytotoxicity, superoxide radical scavenging and molecular docking studies of copper(II) complexes containing N-benzyl-N′-aryl-N″-benzoylguanidine ligands. *Inorg. Chem. Front.* **2015**, *2*, 780−798.
(79) Thirunavukkarasu, T.; Sparkes, H. A.; Natarajan, K. Quinoline based Pd(II) complexes: Synthesis, characterization and evaluation of DNA/protein binding, molecular docking and *in vitro* anticancer activity. *Inorg. Chim. Acta* **2018**, *482*, 229−239.
(80) Akkoç, S. Antiproliferative activities of 2-hydroxyethyl substituted benzimidazolium salts and their palladium complexes against human cancerous cell lines. *Synth. Commun.* **2019**, *49*, 2903−2914.
(81) Quirante, J.; Ruiz, D.; Gonzalez, A.; López, C.; Cascante, M.; Cortés, R.; Messeguer, R.; Calvis, C.; Baldomà, L.; Pascual, A.; Guérardel, Y.; Pradines, B.; Font-Bardía, M.; Calvet, T.; Biot, C. Platinum(II) and palladium(II) complexes with (N,N′) and (C,N,N′)-ligands derived from pyrazole as anticancer and antimalarial agents: Synthesis, characterization and *in vitro* activities. *J. Inorg. Biochem.* **2011**, *105*, 1720−1728.
(82) Mansouri-Torshizi, H.; Rezaei, E.; Kamranfar, F.; Heidari Majd, M. Investigating the apoptosis ability of ethylenediamine 8-hydroxyquinolinato palladium(II) complex. *Adv. Pharm. Bull.* **2016**, *6*, 449−453.

https://dx.doi.org/10.1021/acs.inorgchem.0c02373
Inorg. Chem. 2020, 59, 17109−17122

(83) Ulukaya, E.; Ari, F.; Dimas, K.; Ikitimur, E. I.; Guney, E.; Yilmaz, V. T. Anti-cancer activity of a novel palladium(II) complex on human breast cancer cells *in vitro* and *in vivo*. *Eur. J. Med. Chem.* **2011**, *46*, 4957−4963.
(84) Montagner, D.; Gandin, V.; Marzano, C.; Erxleben, A. DNA damage and induction of apoptosis in pancreatic cancer cells by a new dinuclear *bis*(triazacyclonane) copper complex. *J. Inorg. Biochem.* **2015**, *145*, 101−107.
(85) Wang, B.; Wang, Z.; Ai, F.; Tang, W. K.; Zhu, G. A monofunctional platinum(II)-based anticancer agent from a salicylanilide derivative: Synthesis, antiproliferative activity, and transcription inhibition. *J. Inorg. Biochem.* **2015**, *142*, 118−125.
(86) Morais, T. S.; Valente, A.; Tomaz, A. I.; Marques, F.; Garcia, M. H. Tracking antitumor metallodrugs: Promising agents with the Ru(II)- and Fe(II)-cyclopentadienyl scaffolds. *Future Med. Chem.* **2016**, *8*, 527−544.
(87) Qi, H.; Lu, J.; Li, J.; Wang, M.; Xu, Y.; Wang, Y.; Zhang, H. Enhanced antitumor activity of monophosphate ester prodrugs of gemcitabine: *In vitro* and *in vivo* evaluation. *J. Pharm. Sci.* **2016**, *105*, 2966−2973.
(88) Crowley, L. C.; Marfell, B. J.; Scott, A. P.; Boughaba, J. A.; Chojnowski, G.; Christensen, M. E.; Waterhouse, N. J. Dead Cert: Measuring cell death. *Cold Spring Harb. Protoc.* **2016**, *2016*, pdb.top070318.
(89) Wu, X. Dual AO/EB staining to detect apoptosis in osteosarcoma cells compared with flow cytometry. *Med. Sci. Monit. Basic Res.* **2015**, *21*, 15−20.
(90) Balakrishnan, N.; Haribabu, J.; Dhanabalan, A. K.; Swaminathan, S.; Sun, S.; Dibwe, D. F.; Bhuvanesh, N.; Awale, S.; Karvembu, R. Thiosemicarbazone(s)-anchored water soluble mono- and bimetallic Cu(II) complexes: Enzyme like activities, biomolecular interactions, anticancer property and real-time live cytotoxicity. *Dalton Trans.* **2020**, *49*, 9411−9424.
(91) Tarnowski, B. I.; Spinale, F. G.; Nicholson, J. H. DAPI as a useful stain for nuclear quantitation. *Biotech. Histochem.* **1991**, *66*, 296−302.
(92) Dmitrieva, N. I.; Burg, M. B. Analysis of DNA breaks, DNA damage response, and apoptosis produced by high NaCl. *Am. J. Physiol. Renal Physiol.* **2008**, *295*, F1678−F1688.
(93) Kalyanaraman, B.; Darley-Usmar, V.; Davies, K. J. A.; Dennery, P. A.; Forman, H. J.; Grisham, M. B.; Mann, G. E.; Moore, K.; Roberts, L. J., II; Ischiropoulos, H. Measuring reactive oxygen and nitrogen species with fluorescent probes: Challenges and limitations. *Free Radical Biol. Med.* **2012**, *52*, 1−6.
(94) Wang, H.; Joseph, J. A. Quantifying cellular oxidative stress by dichlorofluorescein assay using microplate. *Free Radical Biol. Med.* **1999**, *27*, 612−616.
(95) Sellamani, M.; Kalagatur, N. K.; Siddaiah, C.; Mudili, V.; Krishna, K.; Natarajan, G.; Rao Putcha, V. L. Antifungal and zearalenone inhibitory activity of pediococcus pentosaceus isolated from dairy products on fusarium graminearum. *Front. Microbiol.* **2016**, *7*, 890.
(96) Mahmood, T.; Yang, P.-C. Western Blot: Technique, theory, and trouble shooting. *Am. J. Med. Sci.* **2012**, *4*, 429−434.
(97) Nunez, R. DNA measurement and cell cycle analysis by flow cytometry. *Curr. Issues Mol. Biol.* **2001**, *3*, 67−70.
(98) Wang, C.; Shih, W.; Chang, H. C.; Kuo, Y.; Hung, W.; Ong, T.; Li, W. Preparation and characterization of amino-linked heterocyclic carbene palladium, gold, and silver complexes and their use as anticancer agents that act by triggering apoptotic cell death. *J. Med. Chem.* **2011**, *54*, 5245−5249.
(99) Mullard, A. Flooded by the torrent: The COVID-19 drug pipeline. *Lancet* **2020**, *395*, 1245−1246.

https://dx.doi.org/10.1021/acs.inorgchem.0c02373
Inorg. Chem. 2020, 59, 17109−17122